Neutral pion photoproduction on the nucleon in a chiral quark model

Li-Ye Xiao,[1] Xu Cao,[2] and Xian-Hui Zhong[1,*]

[1] *Department of Physics, Hunan Normal University, and Key Laboratory of Low-Dimensional Quantum Structures and Quantum Control of Ministry of Education, Changsha 410081, China*

[2] *Institute of Modern Physics, Chinese Academy of Sciences, Lanzhou 730000, China*

(Received 31 May 2015; revised manuscript received 3 August 2015; published 8 September 2015)

A chiral quark-model approach is adopted to study the $\gamma p \to \pi^0 p$ and $\gamma n \to \pi^0 n$ reactions. Good descriptions of the total and differential cross sections and single-polarization observables are obtained from the pion production threshold up to the second resonance region. It is found that (i) the $n = 0$ shell resonance $\Delta(1232)P_{33}$, the $n = 1$ shell resonances $N(1535)S_{11}$ and $N(1520)D_{13}$, and the $n = 2$ shell resonance $N(1720)P_{13}$ play crucial roles in these two processes. They are responsible for the first, second, and third bump structures in the cross sections, respectively. (ii) Furthermore, obvious evidence of $N(1650)S_{11}$ and $\Delta(1620)S_{31}$ is also found in the reactions. They notably affect the cross sections and the polarization observables from the second resonance region to the third resonance region. (iii) The u-channel background plays a crucial role in the reactions. It has strong interferences with the s-channel resonances. (iv) The t-channel background seems to be needed in the reactions. Including the t-channel vector-meson exchange contribution, the descriptions in the energy region $E_\gamma = 600$–900 MeV are improved significantly. The helicity amplitudes of the main resonances, $\Delta(1232)P_{33}$, $N(1535)S_{11}$, $N(1520)D_{13}$, $N(1720)P_{13}$, $N(1650)S_{11}$, and $\Delta(1620)S_{31}$, are extracted and compared with the results from other groups.

DOI: 10.1103/PhysRevC.92.035202 PACS number(s): 13.60.Le, 14.20.Gk, 12.39.Jh, 12.39.Fe

I. INTRODUCTION

Understanding of the baryon spectrum and searching for the missing nucleon resonances and new exotic states are favored topics in hadronic physics [1]. Photoproduction of mesons is an ideal tool for the study of nucleon and $\Delta(1232)$ spectroscopies in experiments [2]. Neutral pion photoproduction reactions are of special interest because the neutral pions do not couple directly to photons so that nonresonant background contributions are suppressed (i.e., no contact term contribution) [3]. In the past few years, great progress has been achieved in experiments studying the $\gamma p \to \pi^0 p$ reaction at JLab, CB-ELSA, MAMI, and GRAAL. These experimental groups have carried out precise measurements of the differential cross sections and single-polarization observables with a large solid angle coverage and a wide photon energy range [4–15]. Recently they also have finished some measurements of the double-polarization observables [10,16–18]. Furthermore, in recent years significant progress has been achieved in experiments measuring the $\gamma n \to \pi^0 n$ reaction as well. In 2009, some measurements of the beam asymmetries for the $\gamma n \to \pi^0 n$ process were obtained by the GRAAL experiment in the second and third resonances region [19]. Very recently, the quasifree differential and total cross sections in the second and third resonances region for this reaction were also measured by the Crystal Ball/TAPS experiment at MAMI [3]. Thus, improvement of the experimental situations gives us a good opportunity to study the excitation spectroscopies of the nucleon and $\Delta(1232)$.

Stimulated by these new measurements, many partial-wave analysis groups, such as BnGa [20–22], SAID [23–25], MAID [26], Kent [27], Jülich [28,29], and ANL-Osaka [30], have updated their analyses in recent years. For the $\gamma p \to \pi^0 p$ reaction, good descriptions of the data up to the second and third resonances region have been obtained by different groups. However, the explanations of the reaction data and the extracted resonance properties from the reaction still exhibit strong model dependencies. For example, the γp couplings for some well-established resonances, such as $N(1535)S_{11}$, $N(1650)S_{11}$ and $N(1520)D_{13}$, extracted by various groups differ rather notably from each other. For the $\gamma n \to \pi^0 n$ reaction, consistent predictions from different approaches can only be obtained in the first resonance region [3]. Because of the lack of data, the predictions from different models in the second and third resonances region are very different. Fortunately, in this energy region some new measurements of the cross section for the $\gamma n \to \pi^0 n$ reaction at MAMI [3] were reported about one year ago.

These new data for the $\gamma n \to \pi^0 n$ reaction not only provide us a good opportunity to extract more knowledge of the neutron resonances, but also shed light on the puzzle of the narrow structure around $W = 1.68$ GeV observed in the excitation function of η production off quasifree neutrons by several experimental groups [31–33]. This narrow structure has been listed by the Particle Data Group (PDG) as a new nucleon resonance $N(1685)$ [34]. However, many controversial explanations about this narrow structure, such as the $N(1650)S_{11}$ and $N(1710)P_{11}$ coupled-channel effects, interference effects between $N(1650)S_{11}$, $N(1710)P_{11}$, and $N(1720)P_{13}$, and effects from strangeness threshold openings, can be found in the literature [35–37]. In our quark model study, we find that the narrow structure around $W = 1.68$ GeV can be explained by the constructive interference between $N(1535)S_{11}$ and $N(1650)S_{11}$ [38]. Our conclusion is consistent with the analysis from the BnGa group [39,40]. It should be mentioned

*zhongxh@hunnu.edu.cn

TABLE I. The CGLN amplitudes of s-channel resonances in the $n \leqslant 2$ shell for the $\gamma p \to \pi^0 p$ process in the SU(6)⊗O(3) symmetry limit. We have defined $A \equiv -(\frac{\omega_m}{E_f+M_N}+1)|\mathbf{q}|$, $B \equiv \frac{\omega_m}{\mu_q}+\frac{2|\mathbf{q}|}{3\alpha^2}A$, $C \equiv \frac{\omega_m}{\mu_q}+\frac{|\mathbf{q}|}{\alpha^2}A$, $D \equiv \frac{\omega_m}{\mu_q}+\frac{2|\mathbf{q}|}{5\alpha^2}A$, $x \equiv \frac{|\mathbf{k}||\mathbf{q}|}{3\alpha^2}$, $P_l'(z) \equiv \frac{\partial P_l(z)}{\partial z}$, and $P_l''(z) \equiv \frac{\partial^2 P_l(z)}{\partial z^2}$. The ω_γ, ω_m, and E_f stand for the energies of the incoming photon, outgoing meson, and final nucleon, respectively. m_q is the constituent u or d quark mass. $1/\mu_q$ is a factor defined by $1/\mu_q = 2/m_q$. $P_l(z)$ is the Legendre function with $z = \cos\theta$.

Resonance	$[N_6,{}^{2S+1}N_3,n,l]$	f_1^R	f_2^R	f_3^R	f_4^R
$N(938)P_{11}$	$[56,{}^28,0,0]$	0	$+i\frac{5\sqrt{2}}{2}\frac{k}{6m_q}A$	0	0
$\Delta(1232)P_{33}$	$[56,{}^410,0,0]$	$+i\frac{4\sqrt{2}}{3}\frac{k}{6m_q}AP_2'(z)$	$+i\frac{8\sqrt{2}}{3}\frac{k}{6m_q}A$	$-i\frac{4\sqrt{2}}{3}\frac{k}{6m_q}AP_2''(z)$	0
$N(1535)S_{11}$	$[70,{}^28,1,1]$	$-i\frac{\sqrt{2}}{18}k(1+\frac{k}{2m_q})B$	0	0	0
$\Delta(1620)S_{31}$	$[70,{}^210,1,1]$	$+i\frac{\sqrt{2}}{36}k(1-\frac{k}{6m_q})B$	0	0	0
$N(1520)D_{13}$	$[70,{}^28,1,1]$	$+i\frac{\sqrt{2}}{27}k(1+\frac{k}{2m_q})\frac{\lvert\mathbf{q}\rvert}{\alpha^2}A$	$+i\frac{\sqrt{2}}{54}k\frac{k}{m_q}\frac{\lvert\mathbf{q}\rvert}{\alpha^2}AP_2'(z)$	0	$-i\frac{\sqrt{2}}{27}k\frac{\lvert\mathbf{q}\rvert}{\alpha^2}AP_2''(z)$
$\Delta(1700)D_{33}$	$[70,{}^210,1,1]$	$-i\frac{\sqrt{2}}{54}k(1-\frac{k}{6m_q})\frac{\lvert\mathbf{q}\rvert}{\alpha^2}A$	$+i\frac{\sqrt{2}}{54}k\frac{k}{6m_q}\frac{\lvert\mathbf{q}\rvert}{\alpha^2}AP_2'(z)$	0	$+i\frac{\sqrt{2}}{54}k\frac{\lvert\mathbf{q}\rvert}{\alpha^2}AP_2''(z)$
$N(1440)P_{11}$	$[56,{}^28,2,0]$	0	$+i\frac{11\sqrt{2}}{36\times18}\frac{15}{19}k\frac{k}{m_q}Cx$	0	0
$N(1710)P_{11}$	$[70,{}^28,2,0]$	0	$+i\frac{11\sqrt{2}}{36\times18}\frac{6}{19}k\frac{k}{m_q}Cx$	0	0
$\Delta(1750)P_{31}$	$[70,{}^210,2,0]$	0	$-i\frac{11\sqrt{2}}{36\times18}\frac{2}{19}k\frac{k}{m_q}Cx$	0	0
$N(1720)P_{13}$	$[56,{}^28,2,2]$	$-i\frac{\sqrt{2}}{90}\frac{25}{12}k(1+\frac{k}{2m_q})DP_2'(z)x$	$-i\frac{\sqrt{2}}{90}\frac{25}{12}k\frac{k}{2m_q}Dx$	$-i\frac{\sqrt{2}}{90}\frac{25}{12}kDP_2''(z)x$	0
$N(1900)P_{13}$	$[70,{}^28,2,2]$	$-i\frac{\sqrt{2}}{90}\frac{10}{12}k(1+\frac{k}{2m_q})DP_2'(z)x$	$-i\frac{\sqrt{2}}{90}\frac{10}{12}k\frac{k}{2m_q}Dx$	$-i\frac{\sqrt{2}}{90}\frac{10}{12}kDP_2''(z)x$	0
$\Delta(1985?)P_{33}$	$[70,{}^210,2,2]$	$+i\frac{\sqrt{2}}{90}\frac{5}{12}k(1-\frac{k}{6m_q})DP_2'(z)x$	$-i\frac{\sqrt{2}}{90}\frac{5}{12}k\frac{k}{6m_q}Dx$	$+i\frac{\sqrt{2}}{90}\frac{5}{12}kDP_2''(z)x$	0
$\Delta(1920)P_{33}$	$[56,{}^410,2,2]$	0	$-i\frac{\sqrt{2}}{90}\frac{10}{9}k\frac{k}{2m_q}Dx$	$+i\frac{\sqrt{2}}{90}\frac{10}{9}k\frac{k}{2m_q}DP_2''(z)x$	0
$\Delta(1600)P_{33}$	$[56,{}^410,2,0]$	$+i\frac{\sqrt{2}}{90}\frac{10}{9}k\frac{k}{2m_q}CP_2'(z)x$	$+i\frac{\sqrt{2}}{90}\frac{20}{9}k\frac{k}{2m_q}Cx$	$-i\frac{\sqrt{2}}{90}\frac{10}{9}k\frac{k}{2m_q}CP_2''(z)x$	0
$\Delta(1905)F_{35}$	$[56,{}^410,2,2]$	$+i\frac{2\sqrt{2}}{3}\frac{5k}{630m_q}AP_2'(z)x^2$	$+i\frac{2\sqrt{2}}{3}\frac{2k}{630m_q}AP_3'(z)x^2$	$+i\frac{2\sqrt{2}}{3}\frac{3k}{630m_q}AP_2''(z)x^2$	$-i\frac{2\sqrt{2}}{3}\frac{3k}{630m_q}AP_3''(z)x^2$
$\Delta(?)F_{35}$	$[70,{}^210,2,2]$	$-i\frac{\sqrt{2}}{180}(1-\frac{k}{6m_q})AP_2'(z)x^2$	$+i\frac{\sqrt{2}}{180}\frac{k}{6m_q}AP_3'(z)x^2$	$-i\frac{\sqrt{2}}{180}AP_2''(z)x^2$	$+i\frac{\sqrt{2}}{180}AP_3''(z)x^2$
$N(1680)F_{15}$	$[56,{}^28,2,2]$	$+i\frac{5\sqrt{2}}{180}(1+\frac{k}{2m_q})AP_2'(z)x^2$	$+i\frac{5\sqrt{2}}{180}\frac{k}{2m_q}AP_3'(z)x^2$	$+i\frac{5\sqrt{2}}{180}AP_2''(z)x^2$	$-i\frac{5\sqrt{2}}{180}AP_3''(z)x^2$
$N(?)F_{15}$	$[70,{}^28,2,2]$	$+i\frac{2\sqrt{2}}{180}(1+\frac{k}{2m_q})AP_2'(z)x^2$	$+i\frac{2\sqrt{2}}{180}\frac{k}{2m_q}AP_3'(z)x^2$	$+i\frac{2\sqrt{2}}{180}AP_2''(z)x^2$	$-i\frac{2\sqrt{2}}{180}AP_3''(z)x^2$
$\Delta(1950)F_{37}$	$[56,{}^410,2,2]$	$+i\frac{2\sqrt{2}}{3}\frac{k}{70m_q}AP_4'(z)x^2$	$+i\frac{2\sqrt{2}}{3}\frac{2k}{105m_q}AP_3'(z)x^2$	$-i\frac{2\sqrt{2}}{3}\frac{k}{210m_q}AP_4''(z)x^2$	$+i\frac{2\sqrt{2}}{3}\frac{k}{210m_q}AP_3''(z)x^2$

that the γn coupling for $N(1650)S_{11}$ extracted by us and the BnGa group has a positive sign, which is opposite to that of the PDG [34]. Now, two questions arise naturally: (i) Can some clues about the controversially discussed $N(1685)$ be found in the $\gamma n \to \pi^0 n$ reaction? (ii) Are the properties of $N(1535)S_{11}$ and $N(1650)S_{11}$ extracted from the ηN channel consistent with those extracted from the $\pi^0 N$ channel? To better understand these questions, a systematic analysis of the recent data for neutral pion production off nucleons is urgently needed.

In this work, we carry out a combined study of the $\gamma p \to \pi^0 p$ and $\gamma n \to \pi^0 n$ reactions in a chiral quark model. By systematically analyzing the new data for neutral pion photoproduction on the nucleons, we attempt to uncover some puzzles existing in the photoproduction reactions and obtain a better understanding of the excitation spectra of the nucleon and $\Delta(1232)$. It should be mentioned that there are interesting differences between $\gamma p \to \pi^0 p$ and $\gamma n \to \pi^0 n$. In the γp reactions, contributions from the nucleon resonances of representation $[70,{}^48]$ will be suppressed by the Moorhouse selection rule [41,42]. In contrast, all the octet states can contribute to the γn reactions. In other words, more states will be present in the γn reactions. Therefore, by studying neutral pion photoproduction on nucleons, we expect that the role played by intermediate baryon resonances can be highlighted.

In the chiral quark model, an effective chiral Lagrangian is introduced to account for the quark-pseudoscalar-meson coupling. Since the quark-meson coupling is invariant under the chiral transformation, some of the low-energy properties of QCD are retained. The chiral quark model has been well developed and widely applied to meson photoproduction reactions [38,43–54]. Recently, this model has been successfully extended to πN and KN reactions as well [55–58].

The paper is organized as follows. In Sec. II, a brief review of the chiral quark model approach is given. The numerical results are presented and discussed in Sec. III. Finally, a summary is given in Sec. IV.

II. THE MODEL

In this section, we give a brief review of the chiral quark model. In this model, the s- and u-channel transition amplitudes are determined by [44,45]

$$\mathcal{M}_s = \sum_j \langle N_f|H_m|N_j\rangle\langle N_j|\frac{1}{E_i+\omega_\gamma-E_j}H_e|N_i\rangle, \quad (1)$$

$$\mathcal{M}_u = \sum_j \langle N_f|H_e\frac{1}{E_i-\omega_m-E_j}|N_j\rangle\langle N_j|H_m|N_i\rangle, \quad (2)$$

where H_m and H_e stand for the quark-pseudoscalar-meson and electromagnetic couplings at the tree level, respectively. They

TABLE II. The CGLN amplitudes of s-channel resonances in the $n \leqslant 2$ shell for the $\gamma n \to \pi^0 n$ process in the SU(6)⊗O(3) symmetry limit.

Resonance	$[N_6,{}^{2S+1}N_3,n,l]$	f_1^R	f_2^R	f_3^R	f_4^R
$N(940)P_{11}$	$[56,{}^28,0,0]$	0	$+i\frac{5\sqrt{2}}{3}\frac{k}{6m_q}A$	0	0
$\Delta(1232)P_{33}$	$[56,{}^410,0,0]$	$+i\frac{4\sqrt{2}}{3}\frac{k}{6m_q}AP_2'(z)$	$+i\frac{8\sqrt{2}}{3}\frac{k}{6m_q}A$	$-i\frac{4\sqrt{2}}{3}\frac{k}{6m_q}AP_2''(z)$	0
$N(1535)S_{11}$	$[70,{}^28,1,1]$	$-i\frac{\sqrt{2}}{18}k(1+\frac{k}{6m_q})B$	0	0	0
$N(1650)S_{11}$	$[70,{}^48,1,1]$	$+i\frac{\sqrt{2}}{36}k\frac{k}{6m_q}B$	0	0	0
$\Delta(1620)S_{31}$	$[70,{}^210,1,1]$	$+i\frac{\sqrt{2}}{36}k(1-\frac{k}{6m_q})B$	0	0	0
$N(1520)D_{13}$	$[70,{}^28,1,1]$	$+i\frac{\sqrt{2}}{9}(1+\frac{k}{6m_q})Ax$	$+i\frac{\sqrt{2}}{9}\frac{k}{6m_q}AxP_2'(z)$	0	$-i\frac{\sqrt{2}}{9}AxP_2''(z)$
$N(1700)D_{13}$	$[70,{}^48,1,1]$	$+i\frac{\sqrt{2}}{18}\frac{4}{5}\frac{k}{6m_q}Ax$	$+i\frac{\sqrt{2}}{18}\frac{1}{5}\frac{k}{6m_q}AxP_2'(z)$	0	$-i\frac{\sqrt{2}}{18}\frac{3}{5}\frac{k}{6m_q}AxP_2''(z)$
$\Delta(1700)D_{33}$	$[70,{}^210,1,1]$	$-i\frac{\sqrt{2}}{18}(1-\frac{k}{6m_q})Ax$	$+i\frac{\sqrt{2}}{18}\frac{k}{6m_q}AxP_2'(z)$	0	$+i\frac{\sqrt{2}}{18}AxP_2''(z)$
$N(1675)D_{15}$	$[70,{}^48,1,1]$	$+i\frac{\sqrt{2}}{6}\frac{k}{15m_q}AxP_3'(z)$	$+i\frac{\sqrt{2}}{6}\frac{k}{10m_q}AxP_2'(z)$	$-i\frac{\sqrt{2}}{6}\frac{k}{2m_q}Axz$	$+i\frac{\sqrt{2}}{6}\frac{k}{30m_q}AxP_2''(z)$
$N(1440)P_{11}$	$[56,{}^28,2,0]$	0	$+i\frac{47\sqrt{2}}{36\times108}\frac{10}{11}k\frac{k}{m_q}Cx$	0	0
$N(1710)P_{11}$	$[70,{}^28,2,0]$	0	$+i\frac{47\sqrt{2}}{36\times108}\frac{2}{11}k\frac{k}{m_q}Cx$	0	0
$\Delta(1750)P_{31}$	$[70,{}^210,2,0]$	0	$-i\frac{47\sqrt{2}}{36\times108}\frac{1}{11}k\frac{k}{m_q}Cx$	0	0
$N(?)P_{11}$	$[70,{}^48,2,2]$	0	$-i\frac{47\sqrt{2}}{36\times108}\frac{1}{9}k\frac{k}{m_q}Dx$	0	0
$\Delta(1910)P_{31}$	$[56,{}^410,2,2]$	0	$-i\frac{47\sqrt{2}}{36\times108}\frac{8}{9}k\frac{k}{m_q}Dx$	0	0
$N(1720)P_{13}$	$[56,{}^28,2,2]$	$-i\frac{\sqrt{2}}{108}\frac{10}{2}k\frac{k}{6m_q}DP_2'(z)x$	$-i\frac{\sqrt{2}}{108}\frac{10}{2}k\frac{k}{6m_q}Dx$	0	0
$N(1900)P_{13}$	$[70,{}^28,2,2]$	$-i\frac{\sqrt{2}}{108}k(1+\frac{k}{6m_q})DP_2'(z)x$	$-i\frac{\sqrt{2}}{108}k\frac{k}{6m_q}Dx$	$-i\frac{\sqrt{2}}{108}kDP_2''(z)x$	0
$N(?)P_{13}$	$[70,{}^48,2,2]$	0	$-i\frac{\sqrt{2}}{108}\frac{1}{2}k\frac{k}{6m_q}Dx$	$+i\frac{\sqrt{2}}{108}\frac{1}{2}k\frac{k}{6m_q}DP_2''(z)x$	0
$\Delta(1985?)P_{33}$	$[70,{}^210,2,2]$	$+i\frac{\sqrt{2}}{108}\frac{1}{2}k(1-\frac{k}{6m_q})DP_2'(z)x$	$-i\frac{\sqrt{2}}{108}\frac{1}{2}k\frac{k}{6m_q}Dx$	$+i\frac{\sqrt{2}}{108}\frac{1}{2}kDP_2''(z)x$	0
$\Delta(1920)P_{33}$	$[56,{}^410,2,2]$	0	$-i\frac{\sqrt{2}}{108}\frac{8}{2}k\frac{k}{6m_q}Dx$	$+i\frac{\sqrt{2}}{108}\frac{8}{2}k\frac{k}{6m_q}DP_2''(z)x$	0
$\Delta(1600)P_{33}$	$[56,{}^410,2,0]$	$+i\frac{\sqrt{2}}{108}\frac{8}{2}k\frac{k}{6m_q}CP_2'(z)x$	$+i\frac{\sqrt{2}}{108}\frac{24}{2}k\frac{k}{6m_q}Cx$	$-i\frac{\sqrt{2}}{108}\frac{16}{2}k\frac{k}{6m_q}CP_2''(z)x$	0
$N(?)P_{13}$	$[70,{}^48,2,0]$	$+i\frac{\sqrt{2}}{108}\frac{1}{2}k\frac{k}{6m_q}CP_2'(z)x$	$+i\frac{\sqrt{2}}{108}\frac{3}{2}k\frac{k}{6m_q}Cx$	$-i\frac{\sqrt{2}}{108}\frac{2}{2}k\frac{k}{6m_q}CP_2''(z)x$	0
$N(1680)F_{15}$	$[56,{}^28,2,2]$	$+i\frac{\sqrt{2}}{18}\frac{k}{6m_q}AP_2'(z)x^2$	$+i\frac{\sqrt{2}}{18}\frac{k}{6m_q}AP_3'(z)x^2$	0	0
$N(?)F_{15}$	$[70,{}^28,2,2]$	$+i\frac{\sqrt{2}}{18}\frac{1}{5}(1+\frac{k}{6m_q})AP_2'(z)x^2$	$+i\frac{\sqrt{2}}{18}\frac{1}{5}\frac{k}{6m_q}AP_3'(z)x^2$	$+i\frac{\sqrt{2}}{18}\frac{1}{5}AP_2''(z)x^2$	$-i\frac{\sqrt{2}}{18}\frac{1}{5}AP_3''(z)x^2$
$N(?)F_{15}$	$[70,{}^48,2,2]$	$+i\frac{\sqrt{2}}{18}\frac{1}{14}\frac{k}{6m_q}AP_2'(z)x^2$	$+i\frac{\sqrt{2}}{18}\frac{1}{35}\frac{k}{6m_q}AP_3'(z)x^2$	$+i\frac{\sqrt{2}}{18}\frac{3}{70}\frac{k}{6m_q}AP_2''(z)x^2$	$-i\frac{\sqrt{2}}{18}\frac{3}{70}\frac{k}{6m_q}AP_3''(z)x^2$
$\Delta(?)F_{35}$	$[70,{}^210,2,2]$	$-i\frac{\sqrt{2}}{18}\frac{1}{10}(1-\frac{k}{6m_q})AP_2'(z)x^2$	$+i\frac{\sqrt{2}}{18}\frac{1}{10}\frac{k}{6m_q}AP_3'(z)x^2$	$-i\frac{\sqrt{2}}{18}\frac{1}{10}AP_2''(z)x^2$	$+i\frac{\sqrt{2}}{18}\frac{1}{10}AP_3''(z)x^2$
$\Delta(1905)F_{35}$	$[56,{}^410,2,2]$	$i\frac{\sqrt{2}}{18}\frac{4}{7}\frac{k}{6m_q}AP_2'(z)x^2$	$+i\frac{\sqrt{2}}{18}\frac{8}{35}\frac{k}{6m_q}AP_3'(z)x^2$	$+i\frac{\sqrt{2}}{18}\frac{12}{35}\frac{k}{6m_q}AP_2''(z)x^2$	$-i\frac{\sqrt{2}}{18}\frac{12}{35}\frac{k}{6m_q}AP_3''(z)x^2$
$\Delta(1950)F_{37}$	$[56,{}^410,2,2]$	$+i\frac{3\sqrt{2}}{4}\frac{8}{9}\frac{k}{70m_q}AP_4'(z)x^2$	$+i\frac{3\sqrt{2}}{4}\frac{8}{9}\frac{2k}{105m_q}AP_3'(z)x^2$	$-i\frac{3\sqrt{2}}{4}\frac{8}{9}\frac{k}{210m_q}AP_4''(z)x^2$	$+i\frac{3\sqrt{2}}{4}\frac{8}{9}\frac{k}{210m_q}AP_3''(z)x^2$
$N(1990)F_{17}$	$[70,{}^48,2,2]$	$+i\frac{3\sqrt{2}}{4}\frac{1}{9}\frac{k}{70m_q}AP_4'(z)x^2$	$+i\frac{3\sqrt{2}}{4}\frac{1}{9}\frac{2k}{105m_q}AP_3'(z)x^2$	$-i\frac{3\sqrt{2}}{4}\frac{1}{9}\frac{k}{210m_q}AP_4''(z)x^2$	$+i\frac{3\sqrt{2}}{4}\frac{1}{9}\frac{k}{210m_q}AP_3''(z)x^2$

are described by [44–46]

$$H_m = \sum_j \frac{1}{f_m}\bar{\psi}_j\gamma_\mu^j\gamma_5^j\psi_j\vec{\tau}\cdot\partial^\mu\vec{\phi}_m, \quad (3)$$

$$H_e = -\sum_j e_j\gamma_\mu^j A^\mu(\mathbf{k},\mathbf{r}), \quad (4)$$

where ψ_j represents the jth quark field in a hadron, ϕ_m is the field of the pseudoscalar-meson octet, and f_m is the meson's decay constant. The ω_γ is the energy of the incoming photons. The $|N_i\rangle$, $|N_j\rangle$, and $|N_f\rangle$ stand for the initial, intermediate, and final states, respectively, and their corresponding energies are E_i, E_j, and E_f, which are the eigenvalues of the nonrelativistic constituent quark model Hamiltonian $\hat{H}$ [59–61]. The s- and u-channel transition amplitudes have been worked out in the harmonic oscillator basis in Refs. [44–46].

The t-channel contributions of vector meson exchange are included in this work. The effective Lagrangians for the vector meson exchange for the $\gamma\pi V$ and Vqq couplings are adopted as [46]

$$\mathcal{L}_{\gamma\pi V} = e\frac{g_{V\pi\gamma}}{m_\pi}\varepsilon_{\alpha\beta\gamma\delta}\partial^\alpha A^\beta\partial^\gamma V^\delta\pi, \quad (5)$$

$$\mathcal{L}_{Vqq} = g_{Vqq}\bar{\psi}_j\left(\gamma_\mu + \frac{\kappa_q}{2m_q}\sigma_{\mu\nu}\partial^\nu\right)V^\mu\psi_j, \quad (6)$$

TABLE III. 450 data points of differential cross section, and 53 data points of total cross section of $\gamma p \to \pi^0 p$ included in our fits. The χ^2 datum point is about $\chi^2/N_{\rm data} = 4.3$.

Data Refs.	Obser.	E_γ	$N_{\rm data}$	χ_i^2	$\chi_i^2/N_{\rm data}$
[4] MAMI	$d\sigma/d\Omega$	240,260,278	27	357	13.2
[5] MAMI	$d\sigma/d\Omega$	300–400	112	540	4.8
[9] CB-ELSA	$d\sigma/d\Omega$	438–862	311	1204	3.9
[72] MAMI	σ	240–335	20	10	0.5
[9] CB-ELSA	σ	342–1138	33	37	1.1

TABLE IV. The strength parameters C_R determined by the experimental data.

C_R parameter	$\gamma p \to \pi^0 p$	$\gamma n \to \pi^0 n$
$C_{S_{11}(1535)}^{[70,^2 8]}$	$0.61^{+0.06}_{-0.04}$	$0.43^{+0.09}_{-0.09}$
$C_{S_{11}(1535)}^{[70,^4 8]}$		-0.42
$C_{S_{11}(1650)}^{[70,^2 8]}$	$0.39^{+0.04}_{-0.06}$	$0.27^{+0.06}_{-0.06}$
$C_{S_{11}(1650)}^{[70,^4 8]}$		1.12
$C_{D_{13}(1520)}^{[70,^2 8]}$	$1.41^{+0.15}_{-0.09}$	$1.32^{+0.09}_{-0.09}$
$C_{D_{13}(1520)}^{[70,^4 8]}$		-1.05
$C_{D_{13}(1700)}^{[70,^2 8]}$	0.09	0.08
$C_{D_{13}(1700)}^{[70,^4 8]}$		2.05
$C_{P_{33}(1232)}$	$1.83^{+0.02}_{-0.04}$	1.83
$C_{S_{31}(1620)}$	$1.80^{+0.50}_{-0.20}$	1.80
$C_{D_{15}(1675)}$	1.00	1.00
$C_{P_{13}(1720)}$	1.00	$3.20^{+0.1}_{-0.2}$

where A and V denote the photon and vector-meson fields, respectively; π stands for the π-meson field; $g_{V\pi\gamma}$ and g_{Vqq} are the coupling constants. The t-channel transition amplitude has been given in the harmonic oscillator basis in Ref. [46].

It should be remarked that the amplitudes in terms of the harmonic oscillator principle quantum number n are the sum of a set of SU(6) multiplets with the same n. To obtain the contributions of individual resonances, we need to separate out the single-resonance-excitation amplitudes within each principle number n in the s channel. Taking into account the width effects of the resonances, the resonance transition amplitudes of the s channel can be generally expressed as [45]

$$\mathcal{M}_R^s = \frac{2M_R}{s - M_R^2 + iM_R\Gamma_R}\mathcal{O}_R e^{-(\mathbf{k}^2+\mathbf{q}^2)/6\alpha^2}, \tag{7}$$

where $\sqrt{s} = E_i + \omega_\gamma$ is the total energy of the system, α is the harmonic oscillator strength, M_R is the mass of the s-channel resonance with a width Γ_R, and $\mathcal{O}_R$ is the separated operators for individual resonances in the s-channel. In the Chew-Goldberger-Low-Nambu (CGLN) parameterization, the transition amplitude can be written in a standard form [62]

$$\mathcal{O}_R = if_1^R \boldsymbol{\sigma}\cdot\boldsymbol{\epsilon} + f_2^R\frac{(\boldsymbol{\sigma}\cdot\mathbf{q})\boldsymbol{\sigma}\cdot(\mathbf{k}\times\boldsymbol{\epsilon})}{|\mathbf{q}||\mathbf{k}|} + if_3^R\frac{(\boldsymbol{\sigma}\cdot\mathbf{k})(\mathbf{q}\cdot\boldsymbol{\epsilon})}{|\mathbf{q}||\mathbf{k}|} + if_4^R\frac{(\boldsymbol{\sigma}\cdot\mathbf{q})(\mathbf{q}\cdot\boldsymbol{\epsilon})}{|\mathbf{q}|^2}, \tag{8}$$

where $\boldsymbol{\sigma}$ is the spin operator of the nucleon, $\boldsymbol{\epsilon}$ is the polarization vector of the photon, and $\mathbf{k}$ and $\mathbf{q}$ are incoming photon and outgoing meson momenta, respectively. In the SU(6)⊗O(3) symmetry limit, we have extracted the CGLN amplitudes for the s-channel resonances in the $n \leqslant 2$ shell for the $\gamma p \to \pi^0 p$ and $\gamma n \to \pi^0 n$ processes, which have been listed in Tables I and II, respectively. Comparing the CGLN amplitudes of different resonances with each other, one can easily find which states are the main contributors to the reactions in the SU(6)⊗O(3) symmetry limit.

Finally, the differential cross section $d\sigma/d\Omega$, photon beam asymmetry Σ, polarization of recoil protons P, and target asymmetry T are given by the following standard expressions [2,63,64]:

$$\frac{d\sigma}{d\Omega} = \frac{\alpha_e\alpha_\pi(E_i+M_N)(E_f+M_N)}{16sM_N^2}\frac{1}{2}\frac{|\mathbf{q}|}{|\mathbf{k}|}\sum_{i=1}^4 |H_i|^2, \tag{9}$$

$$\Sigma = 2\,\mathrm{Re}(H_4^*H_1 - H_3^*H_2)\Big/\sum_{i=1}^4 |H_i|^2, \tag{10}$$

$$P = -2\,\mathrm{Im}(H_4^*H_2 + H_3^*H_1)\Big/\sum_{i=1}^4 |H_i|^2, \tag{11}$$

$$T = 2\,\mathrm{Im}(H_2^*H_1 + H_4^*H_3)\Big/\sum_{i=1}^4 |H_i|^2, \tag{12}$$

where the transition amplitudes H_i in the helicity space can be expressed by the CGLN amplitudes f_i [63]:

$$H_1 = -\frac{1}{\sqrt{2}}\sin\theta\cos\frac{\theta}{2}(f_3+f_4), \tag{13}$$

$$H_2 = \sqrt{2}\cos\frac{\theta}{2}\left[(f_2-f_1)+\sin^2\frac{\theta}{2}(f_3-f_4)\right], \tag{14}$$

$$H_3 = \frac{1}{\sqrt{2}}\sin\theta\sin\frac{\theta}{2}(f_3-f_4), \tag{15}$$

$$H_4 = \sqrt{2}\sin\frac{\theta}{2}\left[(f_2+f_1)+\cos^2\frac{\theta}{2}(f_3-f_4)\right]. \tag{16}$$

In Eq. (9), the fine-structure constant α_e is well determined, and the πNN coupling constant α_π is related to the axial vector coupling g_A by the generalized Goldberg-Treiman relation

$$\alpha_\pi = \frac{1}{4\pi}\left(\frac{g_A M_N}{f_\pi}\right)^2 \equiv \frac{g_{\pi NN}^2}{4\pi}. \tag{17}$$

However, the quark model predicts rather large values $g_A = 5/3$ for charged pions and $g_A = 5\sqrt{2}/6$ for neutral pions. In our paper, the coupling α_π is determined by fitting the data.

TABLE V. The masses M_R (MeV) and widths Γ_R (MeV) for the s-channel resonances in the present work compared with the values of Breit-Wigner (BW) and pole parametrizations from PDG14 [34].

Resonance	$(M_R,\Gamma_R)_{\rm Ours}$	$(M_R,\Gamma_R)_{\rm Pole}$	$(M_R,\Gamma_R)_{\rm BW}$
$\Delta(1232)P_{33}$	$1210^{+2}_{-2},98^{+2}_{-2}$	$1210^{+1}_{-1},100^{+2}_{-2}$	$1232^{+2}_{-2},117^{+3}_{-3}$
$N(1535)S_{11}$	$1515^{+5}_{-7},115^{+10}_{-15}$	$1510^{+20}_{-20},170^{+80}_{-80}$	$1535^{+10}_{-10},150^{+25}_{-25}$
$N(1650)S_{11}$	$1660^{+10}_{-20},150^{+30}_{-20}$	$1655^{+15}_{-15},135^{+35}_{-35}$	$1655^{+15}_{-10},140^{+30}_{-30}$
$\Delta(1630)S_{31}$	$1600^{+10}_{-10},135^{+25}_{-15}$	$1600^{+10}_{-10},130^{+10}_{-10}$	$1630^{+30}_{-30},140^{+10}_{-10}$
$N(1520)D_{13}$	$1518^{+5}_{-5},105^{+5}_{-10}$	$1510^{+5}_{-5},110^{+10}_{-5}$	$1515^{+5}_{-5},115^{+10}_{-15}$
$N(1720)P_{13}$	$1685^{+10}_{-5},120^{+5}_{-10}$	$1675^{+15}_{-15},250^{+150}_{-100}$	$1720^{+30}_{-20},250^{+150}_{-100}$

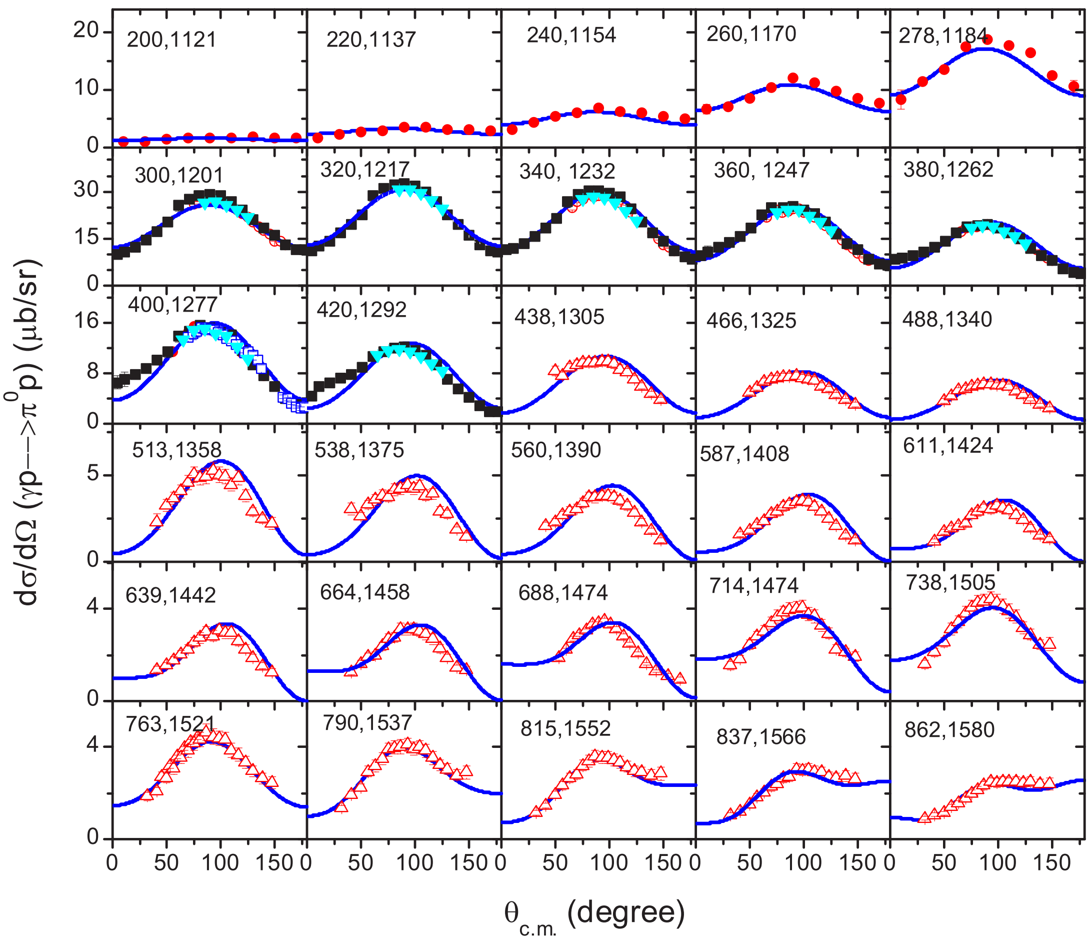

FIG. 1. (Color online) Differential cross section of the $\gamma p \to \pi^0 p$ reaction as a function of scattering angle. Data are taken from [4] (solid circles), [5] (solid squares), [75] (solid triangles), and [9] (open triangles). The first and second numbers in each figure correspond to the photon energy E_γ (MeV) and the πN center-of-mass (c.m.) energy W (MeV), respectively.

III. CALCULATION AND ANALYSIS

A. Parameters

In our framework, the s-channel resonance transition amplitude, $\mathcal{O}_R$, is derived in the SU(6)⊗O(3) symmetry limit. In reality, the SU(6)⊗O(3) symmetry is generally broken due to, e.g., spin-dependent forces in the quark-quark interaction. As a consequence, configuration mixings would occur. The configuration mixings break the SU(6)⊗O(3) symmetry, which can change our theoretical predictions. Furthermore, the helicity couplings and strong decay couplings of some resonances might be over- or underestimated with the simple quark model. To accommodate the uncertainties in the symmetric quark model framework, we introduce a set of coupling strength parameters, C_R, for each resonance amplitude by an empirical method [50–53]:

$$\mathcal{O}_R \to C_R \mathcal{O}_R, \tag{18}$$

where C_R can be determined by fitting the experimental observables. In the SU(6)⊗O(3) symmetry limit, one finds $C_R = 1$, while deviations of C_R from unity imply the SU(6) ⊗ O(3) symmetry breaking.

In our previous study of the η photoproduction on the nucleons, we found the configuration mixings seem to be inevitable for the low-lying S-wave nucleon resonances $N(1535)S_{11}$ and $N(1650)S_{11}$ and D-wave nucleon resonances $N(1520)D_{13}$ and $N(1700)D_{13}$. By including configuration mixing effects in the S- and D-wave states, we explicitly express their transition amplitudes as follows:

$$\mathcal{O}_R \to C_R^{[70,{}^28]} \mathcal{O}_{[70,{}^28,J]} + C_R^{[70,{}^48]} \mathcal{O}_{[70,{}^48,J]}. \tag{19}$$

The coefficients $C_R^{[70,{}^28]}$ and $C_R^{[70,{}^48]}$ can be related to the mixing angles. We adopt the same mixing scheme as in our previous work [38],

$$\begin{pmatrix} S_{11}(1535) \\ S_{11}(1650) \end{pmatrix} = \begin{pmatrix} \cos\theta_S & -\sin\theta_S \\ \sin\theta_S & \cos\theta_S \end{pmatrix} \begin{pmatrix} |70,{}^28,1/2^-\rangle \\ |70,{}^48,1/2^-\rangle \end{pmatrix}, \tag{20}$$

and

$$\begin{pmatrix} D_{13}(1520) \\ D_{13}(1700) \end{pmatrix} = \begin{pmatrix} \cos\theta_D & -\sin\theta_D \\ \sin\theta_D & \cos\theta_D \end{pmatrix} \begin{pmatrix} |70,{}^28,3/2^-\rangle \\ |70,{}^48,3/2^-\rangle \end{pmatrix}. \tag{21}$$

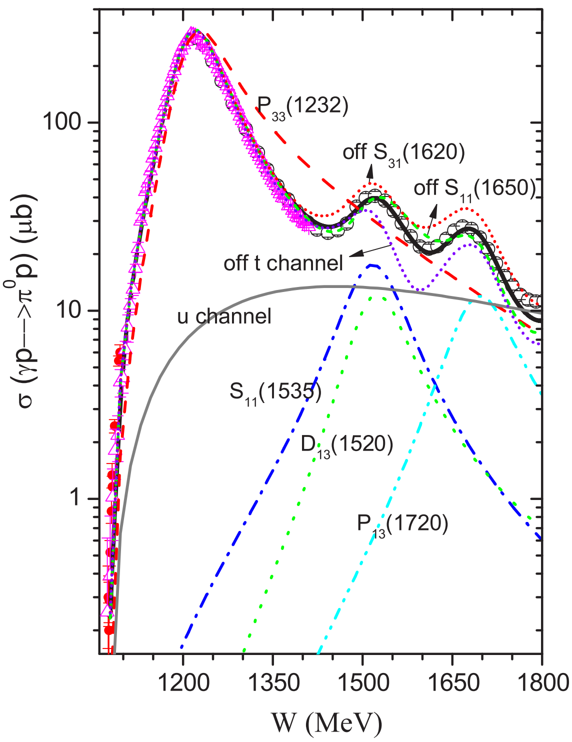

FIG. 2. (Color online) Total cross section as a function of c.m. energy W for the $\gamma p \to \pi^0 p$ reaction. Data are taken from [9] (open circles), [76] (solid circles), and [72] (triangles). The results for switching off the contributions from $N(1650)S_{11}$, $\Delta(1620)S_{31}$, and t channel and the partial cross sections for $\Delta(1232)P_{33}$, $N(1535)S_{11}$, $N(1520)D_{13}$, $N(1720)P_{13}$, and the u channel are indicated explicitly by different legends in the figure.

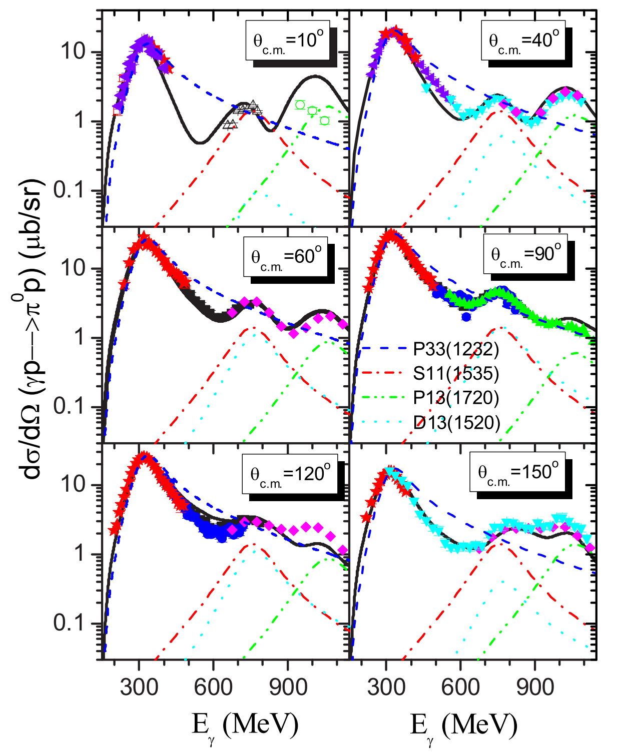

FIG. 3. (Color online) Photon energy dependent differential cross section of the $\gamma p \to \pi^0 p$ reaction. Data are taken from [5] (left triangles), [77] (open squares), [78] (solid stars), [79] (open triangles), [80] (open circles), [81] (solid squares), [82] (solid circles), [9] (down triangles), [11] (up triangles), and [12] (diamonds). The partial cross sections for $\Delta(1232)P_{33}$, $N(1535)S_{11}$, $N(1520)D_{13}$, and $N(1720)P_{13}$ are indicated explicitly by different legends in the figure.

Then, the coefficients defined in Eq. (19) are given by

$$C^{[70,^28]}_{S_{11}(1535)} = R^S_2 \cos\theta_S(\cos\theta_S - \sin\theta_S/2), \quad (22)$$

$$C^{[70,^48]}_{S_{11}(1535)} = R^S_4 \sin\theta_S(\sin\theta_S - 2\cos\theta_S), \quad (23)$$

$$C^{[70,^28]}_{S_{11}(1650)} = R^S_2 \sin\theta_S(\sin\theta_S + \cos\theta_S/2), \quad (24)$$

$$C^{[70,^48]}_{S_{11}(1650)} = R^S_4 \cos\theta_S(\cos\theta_S + 2\sin\theta_S), \quad (25)$$

$$C^{[70,^28]}_{D_{13}(1520)} = R^D_2 \cos\theta_D\left(\cos\theta_D - \frac{1}{2\sqrt{10}}\sin\theta_D\right), \quad (26)$$

$$C^{[70,^48]}_{D_{13}(1520)} = R^D_4 \sin\theta_D(\sin\theta_D - 2\sqrt{10}\cos\theta_D), \quad (27)$$

$$C^{[70,^28]}_{D_{13}(1700)} = R^D_2 \sin\theta_D\left(\sin\theta_D + \frac{1}{2\sqrt{10}}\cos\theta_D\right), \quad (28)$$

$$C^{[70,^48]}_{D_{13}(1700)} = R^D_4 \cos\theta_D(\cos\theta_D + 2\sqrt{10}\sin\theta_D). \quad (29)$$

The parameters R_2 and R_4 are introduced to adjust the overall strength of the partial wave amplitudes of $[70,^28]$ and $[70,^48]$, respectively, which may be overestimated or underestimated in the naive quark model [38]. If $R = 1$, one finds that the C_R parameters of S- and D-wave states can be explained with configuration mixings only. In the calculation, the mixing angle between $N(1535)S_{11}$ and $N(1650)S_{11}$ is adopted to be $\theta_S = 26^\circ$, determined in our previous work [38]. Notice that in our work we have adopted Isgur's later conventions [65] where wave functions are in line with the SU(3) conventions of de Swart [66]. In this frame, we obtain a positive mixing angle θ_S. However, in line with the old conventions of the SU(3) wave functions from Isgur and Karl's early works [59,60], one obtains a negative mixing angle θ_S [50–53,59,67]. This question has been clarified in Refs. [38,68]. Furthermore, the mixing angle between $N(1520)D_{13}$ and $N(1700)D_{13}$ is adopted to be $\theta_D \simeq 10^\circ$ as widely suggested in the literature [51–53,59,67,69].

For the $\gamma p \to \pi^0 p$ reaction, we obtain $R^S_2 \simeq 1.0$ and $R^D_2 \simeq 1.5$ by fitting the 450 data points of differential cross section and the 53 data points of total cross section collected in Table III. For the $\gamma n \to \pi^0 n$ reaction, we obtain $R^S_2 \simeq R^S_4 \simeq 0.7$, $R^D_2 \simeq 1.4$, and $R^D_4 \simeq 1.0$ by fitting the 36 data points of total cross section around the second resonance energy region $1.30 \leqslant W \leqslant 1.72$ GeV recently measured at MAMI [3]. With these determined R parameters, from Eqs. (22)–(29) one can obtain the overall strength parameters $C^{[70,^28]}_R$ and $C^{[70,^48]}_R$ for the S- and D-wave resonances.

The determined C_R values for these low-lying resonances are listed in Table IV. From the table, we find that to reproduce the data we need to introduce two large coupling strength parameters $C_{P_{33}(1232)} \simeq 1.83$ and $C_{S_{31}(1620)} \simeq 1.8$ for $\Delta(1232)P_{33}$ and $\Delta(1620)S_{31}$, respectively. The reason may

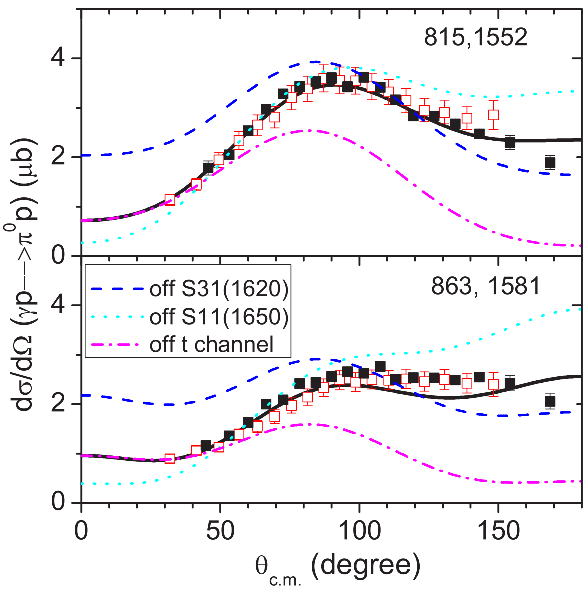

FIG. 4. (Color online) Effects of $N(1650)S_{11}$, $\Delta(1620)S_{31}$, and t channel on the differential cross sections of the $\gamma p \to \pi^0 p$ process. Data are taken from [9] (open squares) and [11] (solid squares). The results by switching off the contributions from $N(1650)S_{11}$, $\Delta(1620)S_{31}$, and t channel are indicated explicitly by different legends in the figure. The first and second numbers in each figure correspond to the photon energy E_γ (MeV) and the πN center-of-mass energy W (MeV), respectively.

be the well-known underestimation of their photocouplings in the constituent quark model [70,71]. We also need to enhance the contributions of $N(1520)D_{13}$ by a factor of $C_{D_{13}(1520)} \simeq 1.4$, which cannot be explained with configuration mixings only. The underestimation of the resonance amplitude of $N(1520)D_{13}$ is also found in the $\gamma N \to \eta N$ processes within the quark model framework [38], which is due to the underestimation of the photocoupling of $N(1520)D_{13}$ in the constituent quark model. In the π^0 photoproduction processes, the data favor a smaller contribution of $N(1535)S_{11}$ than that in the SU(6)⊗O(3) symmetry limit. In the $\gamma p \to \pi^0 p$ reaction, the strength parameter $C^{[70,^28]}_{S_{11}(1535)} \simeq 0.61$ can be naturally explained with the configuration mixings between two S-wave nucleon resonances $N(1535)S_{11}$ and $N(1650)S_{11}$ with a mixing angle $\theta_S \simeq 26^\circ$. However, in the $\gamma n \to \pi^0 n$ reaction, the strength parameter $C^{[70,^28]}_{S_{11}(1535)} \simeq 0.43$ cannot be well explained with the configuration mixing effects only; we should introduce a parameter $R_2^S \simeq 0.7$ to slightly decrease the transition amplitude of $[70,^28,1/2^-]$. Furthermore, we find that in the $\gamma n \to \pi^0 n$ reaction the enhancement of the contributions of $N(1720)P_{13}$ might significantly improve the descriptions of the experimental data.

To take into account relativistic effects, the commonly applied Lorentz boost factor is introduced in the resonance amplitude for the spatial integrals [44], which is

$$\mathcal{O}_R(\mathbf{k},\mathbf{q}) \to \mathcal{O}_R(\gamma_k\mathbf{k},\gamma_q\mathbf{q}), \tag{30}$$

where $\gamma_k = M_N/E_i$ and $\gamma_q = M_N/E_f$.

The πNN coupling α_π and the coupling $g_{\omega\pi\gamma} \cdot g_{\omega qq}$ from ω-meson exchange in the t channel are considered free parameters in the present calculations. By fitting the experimental data of $\gamma p \to \pi^0 p$ reaction (see Table III), we get $g_{\pi NN} \simeq 13.2$ (i.e., $\alpha_\pi \equiv g^2_{\pi NN}/4\pi \simeq 13.8$) and $g_{\omega\pi\gamma} \cdot g_{\omega qq} \simeq 1.37$. The πNN coupling determined in this work is compatible with the value $g_{\pi NN} \simeq 13.5$ adopted in other literature [28,29]. According to the decay of $\omega \to \pi\gamma$, one obtains $g_{\omega\pi\gamma} \simeq 0.32$ [46]. Then the ωqq coupling extracted by us is $g_{\omega qq} \simeq 4.28$, which is consistent with the value $g_{\omega qq} \simeq 3$ suggested in Ref. [73].

There are another two parameters, the constituent quark mass m_q and the harmonic oscillator strength α, from the transition amplitudes. In the calculation we adopt their standard values in the the quark model, $m_q = 330$ MeV and $\alpha^2 = 0.16$ GeV^2.

In the calculations, the $n = 3$ shell resonances are treated as degeneration; their degenerate mass and width are taken as $M = 2080$ MeV and $\Gamma = 200$ MeV, since in the low energy region the contributions from the $n = 3$ shell are not significant. In the u channel, the intermediate states are the nucleon and $\Delta(1232)$ and their resonances. It is found that contributions from the $n \geqslant 1$ shell are negligibly small and insensitive to the degenerate masses for these shells. In this work, we take $M_1 = 1650$ MeV ($M_2 = 1750$ MeV) for the degenerate mass of $n = 1$ ($n = 2$) shell resonances. In the s channel, the masses and widths of the resonances are taken from the PDG [34], or the constituent quark model predictions [61] if no experimental data are available. For the main resonances, we allow their masses and widths to change around the values from the PDG [34] in order to better describe the data. The determined values are listed in Table V. As a comparison, the resonance masses and widths of both pole and Breit-Wigner parametrizations from the PDG [34] are listed in Table V as well. It is found that the resonance masses and widths extracted by us are in good agreement with the values of pole parametrization. The reason is that, when we fit the data, a momentum independent width Γ_R is used, which is similar to the pole parametrization. It should be pointed out that $N(1720)P_{13}$ seems to be a narrow state with a width of 120 MeV in our model, which is about one half of the average value from the PDG [34]. However, our result is in good agreement with that extracted from the $\pi^- p \to K^0\Lambda$ reaction by Saxon *et al.* [74]. The strong decay properties of $N(1720)P_{13}$ will be discussed in detail in another work.

To know some uncertainties of a main parameter (C_R, M_R, Γ_R) we vary it around its central value until the predictions are inconsistent with the data within their uncertainties. The obtained uncertainties for the main parameters have been given in Tables IV and V.

B. $\gamma p \to \pi^0 p$

The chiral quark model studies of $\gamma p \to \pi^0 p$ were carried out in Refs. [43,45,46] about twenty years ago. During the past two decades, great progress has been achieved for pion photoproduction at JLab, CB-ELSA, MAMI, and GRAAL. The new data sets are more accuracy and have larger solid angle coverage and wider photon energy range.

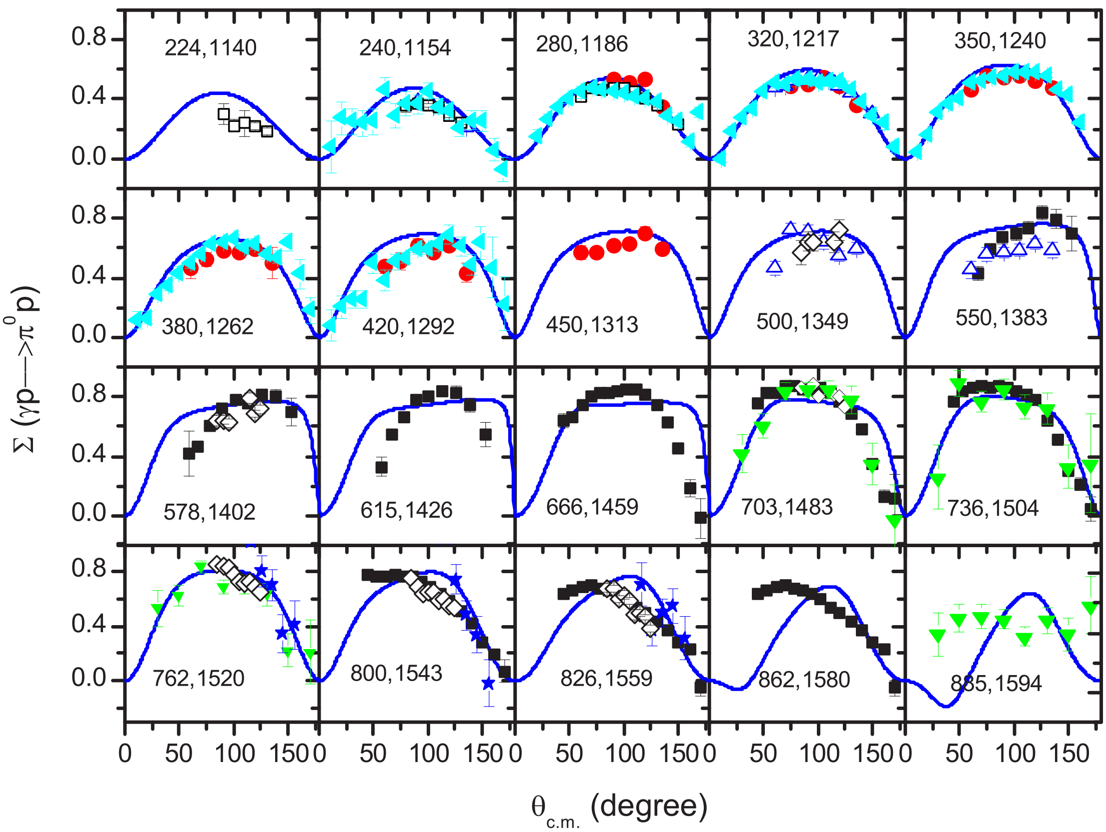

FIG. 5. (Color online) Beam asymmetry of the $\gamma p \to \pi^0 p$ process as a function of scattering angle. The data are taken from [5] (solid left triangles), [83] (open squares), [84] (open up triangles), [85] (solid circles), [11] (solid squares), [13] (diamonds), [86] (solid down triangles), and [14] (stars). The first and second numbers in each figure correspond to the photon energy E_γ (MeV) and the πN center-of-mass energy W (MeV), respectively.

The improvement of the experimental situations gives us a good opportunity to test our model and study the excitation spectra of the nucleon and $\Delta(1232)$ at the same time. All the intermediate states in the s channel classified in the quark model with $n \leqslant 2$ are listed in Table I. It should be pointed out that in this reaction the contributions from the nucleon excitations with the representation $[70,^48]$ are forbidden by the Moorhouse selection rule [41,42]. In the $n = 0$ shell, both nucleon pole and $\Delta(1232)P_{33}$ contribute to the reaction. Comparing their CGLN amplitudes listed in Table I, we can obviously see that $\Delta(1232)P_{33}$ plays a dominant role for its larger amplitudes. In the $n = 1$ shell, two S-wave states $N(1535)S_{11}$ and $\Delta(1620)S_{31}$ and two D-wave states $N(1520)D_{13}$ and $\Delta(1700)D_{33}$ contribute to the reaction. Considering configuration mixing effects, we find that $N(1650)S_{11}$ and $N(1700)D_{13}$ can also contribute to the reaction. Similarly, from Table I we can find that $N(1535)S_{11}$ and $N(1520)D_{13}$ play a dominant role in the $n = 1$ shell S-wave and D-wave resonances, respectively. In the $n = 2$ shell eight P-wave resonances and five F-wave resonances contribute to the reaction. Comparing their CGLN amplitudes we find that $N(1720)P_{13}$ and $N(1680)F_{15}$ play a dominant role in the $n = 2$ shell P-wave resonances and F-wave resonances, respectively.

In present work, we have calculated the differential cross sections, total cross section, beam asymmetry, target asymmetry, and polarization of recoil protons from pion production threshold up to the second resonance region for the $\gamma p \to \pi^0 p$ reaction. The model parameters are determined by fitting the 450 data points of differential cross section from MAMI [4,5] and CB-ELSA [9] in the beam energy region $240 \leqslant E_\gamma \leqslant 862$ MeV, and the 53 data points of total cross section from MAMI [72] and CB-ELSA [9] in the beam energy region $240 \leqslant E_\gamma \leqslant 1138$ MeV (see Table III). The χ^2 datum point is about $\chi^2/N_{\text{data}} = 4.3$. Our results are compared with the data in Figs 1–10.

The differential and total cross sections are shown in Figs. 1 and 2, respectively. It is seen that the chiral quark model can obtain a reasonable description of the data in a wide energy region $E_\gamma = 200$–900 MeV. To clearly see the contributions from different resonances, we also plot the energy dependent differential cross sections in Fig. 3. One can clearly see three bump structures in both the energy dependent differential cross sections and the total cross section. According to our calculations, we find that $\Delta(1232)P_{33}$ is responsible for first bump at $E_\gamma \simeq 300$ MeV. It governs the reaction in the first resonance region. Both $N(1535)S_{11}$ and $N(1520)D_{13}$ together dominate the resonance contributions in the second resonance region. They give approximately equal contributions to the second bump at $E_\gamma \simeq 700$ MeV. The $N(1720)P_{13}$ resonance might be responsible for the third bump at $E_\gamma \simeq 1000$ MeV. It should be mentioned that, although $\Delta(1620)S_{31}$ and $N(1650)S_{11}$ do not give obvious structures in the cross sections, they are crucial to give a correct shape of the differential cross sections from the second resonance region to the third resonance region (see Fig. 4). Switching off their contributions one can see that the total cross sections around $E_\gamma = 700$–1000 MeV are overestimated slightly (see Fig. 2). The u-channel background plays a crucial role in the reaction: it has strong destructive interference with $\Delta(1232)P_{33}$, $N(1535)S_{11}$, and $N(1720)P_{13}$. By including the t-channel vector-meson exchange contribution, we find that the descriptions of the cross sections in the energy region $E_\gamma = 600$–900 MeV are improved notably, while, without the t-channel contributions, the cross sections are underestimated obviously (see Figs. 2 and 4). Finally, it should be mentioned that our quark model explanation of the first and second bump structures in the cross sections are consistent with that of the isobar model [7–9]. However, our quark model explanation of the third bump structure differs from that of the isobar model [7–9]. In Refs. [7–9], the authors predicted that the third bump might be due to three major contributions: $\Delta(1700)D_{33}$, $N(1680)F_{15}$, and $N(1650)S_{11}$, rather than $N(1720)P_{13}$. Thus, to clarify the puzzle about the third bump structure in the cross section more studies of the reaction $\gamma p \to \pi^0 p$ are needed.

The beam asymmetries Σ in the energy region $E_\gamma = 220-900$ MeV are shown in Fig. 5. In this energy region, the polarized data are not as abundant as those of differential cross sections. In the low energy region $E_\gamma < 600$ MeV, until now no data on Σ at forward and backward angles had been obtained. From Fig. 5, it is seen that the chiral quark model has achieved good descriptions of the measured beam asymmetries Σ in the energy region $E_\gamma = 220$–800 MeV. In the higher energy region $E_\gamma > 800$ MeV, it is found that the chiral quark model poorly describes the data at forward angles. To clearly see contributions from different resonances, the energy dependent beam asymmetries at six angles $\theta_{\text{c.m.}} = 20^\circ, 60^\circ, 90^\circ, 125^\circ, 150^\circ, 170^\circ$ are shown in Fig. 6 as well. From the figure, it is found that the beam asymmetry Σ is sensitive to $\Delta(1232)P_{33}$. Its strong effects not only exist in the first resonance region, but also extend to the second resonance region. If we switch off the contributions of $\Delta(1232)P_{33}$, the beam asymmetry Σ changes drastically. Furthermore, we find that both $N(1520)D_{13}$ and $N(1535)S_{11}$ have strong effects on the beam asymmetry Σ around the second resonance region (i.e., $E_\gamma \simeq 700$ MeV), and without their contributions the beam asymmetry Σ in this energy region changes notably. In the higher energy region $E_\gamma > 800$ MeV, it is found that the resonances $\Delta(1232)P_{33}$, $N(1520)D_{13}$, $N(1535)S_{11}$, $N(1650)S_{11}$, $\Delta(1620)S_{31}$, and $N(1720)P_{13}$ together with the u-channel background have equally important contributions to the beam asymmetry Σ. It should be mentioned that when the beam energy $E_\gamma > 800$ MeV, many P- and F-wave states in the $n = 2$ shell begin to have obvious effects on the beam asymmetry Σ as well. Thus, so many equal contributors in this higher energy region make descriptions of the beam asymmetry Σ difficult.

The polarizations of recoil protons P are shown in Fig. 7. In the low energy region $E_\gamma < 650$ MeV, only a few old data with limited angle coverage were obtained. Recently, some precise new data in the higher energy region $E_\gamma \simeq 700$–900 MeV were reported by the CBELSA/TAPS Collaboration [10].

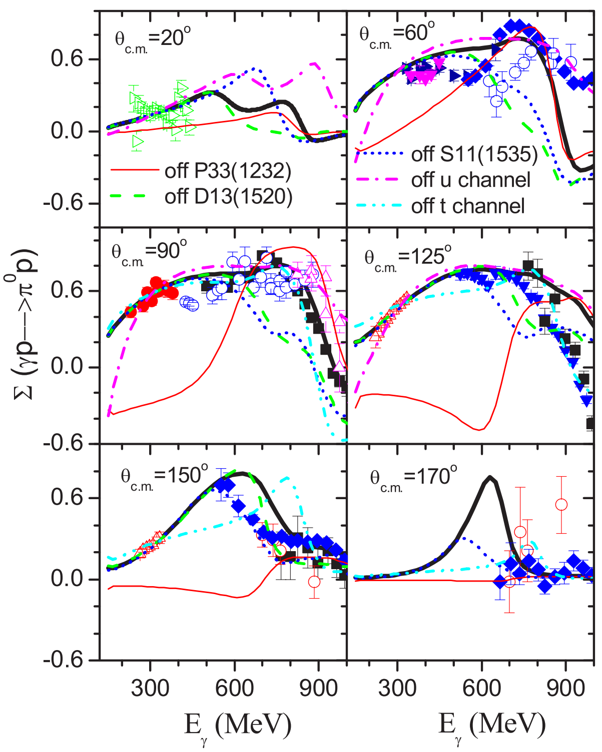

FIG. 6. (Color online) Photon energy dependent beam asymmetry of the $\gamma p \to \pi^0 p$ reaction. The data are taken from [84] (right triangles), [83] (open up triangles), [85] (open diamonds), [11] (solid diamonds), [13] (down triangles), [86] (open circles), [14] (solid squares), [87] (solid circles), and [88] (open squares). The results by switching off the contributions from various partial waves are indicated explicitly by different legends in the figure.

From Fig. 7, it is found that our quark model descriptions are in reasonable agreement with the measurements in a fairly wide energy region $E_\gamma = 280$–800 MeV. Above the photon energy $E_\gamma \simeq 800$ MeV, the quark model descriptions at both forward and backward angles become worse compared with the data. To clearly see contributions from different resonances, the energy dependent P at six angles $\theta_{\text{c.m.}} = 40^\circ, 60^\circ, 90^\circ, 110^\circ, 130^\circ, 150^\circ$ are shown in Fig. 8 as well. It is found that an obvious dip structure appears around $E_\gamma = 700$ MeV, which can be well described in the chiral quark model. The dip structure is due to the strong effects of $\Delta(1232)P_{33}$. When we switch off its contribution, we find that the dip structure disappears. Furthermore, from Fig. 8 it is obviously seen that the polarization of recoil protons P is sensitive to $N(1520)D_{13}$ and $N(1535)S_{11}$ around the second resonance region (i.e., $E_\gamma \simeq 700$ MeV). In the higher energy region $E_\gamma > 800$ MeV, $\Delta(1232)P_{33}$, $N(1520)D_{13}$, $N(1535)S_{11}$, $N(1650)S_{11}$, the u-channel background, and other higher partial waves have approximately equal contributions to P, which leads to a complicated description of the higher energy data.

The target asymmetries T are shown in Fig. 9. Below the photon energy $E_\gamma \simeq 700$ MeV, only a few old data with a very small angle coverage were obtained. Recently, some precise data with larger angle coverage in the higher energy region

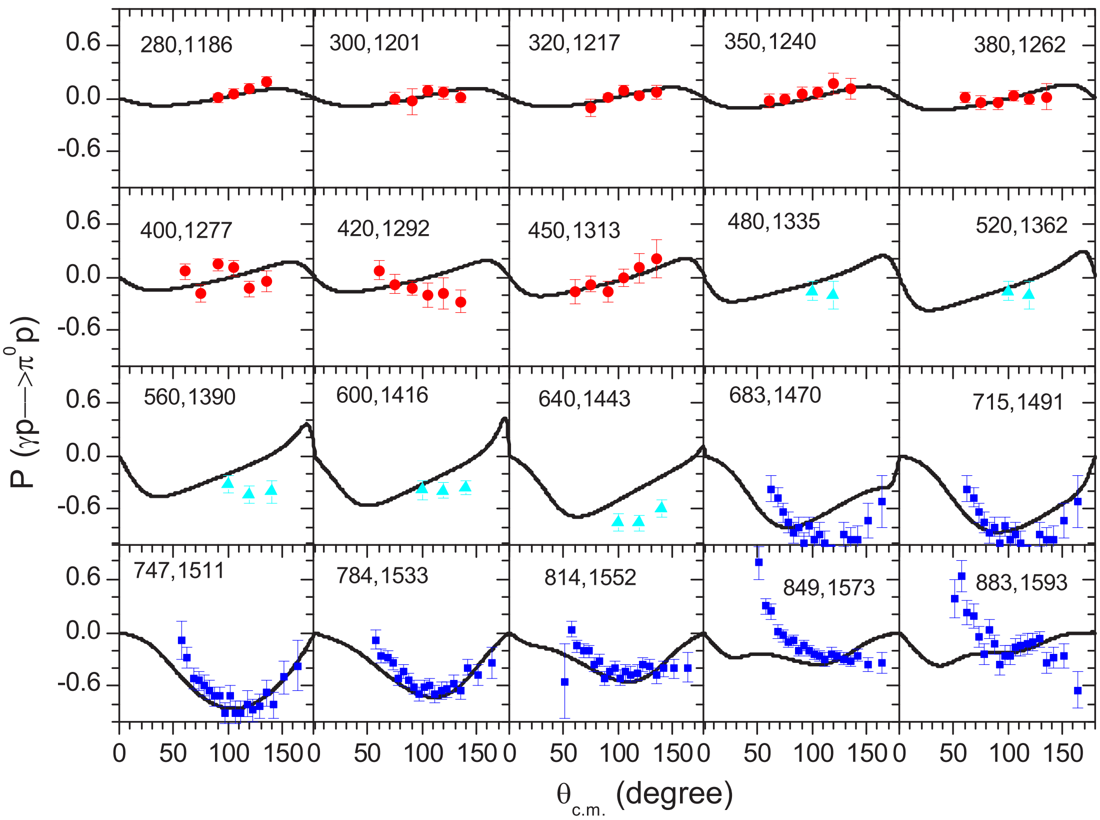

FIG. 7. (Color online) Polarization of recoil protons P of the $\gamma p \to \pi^0 p$ reaction as a function of scattering angle. Data are taken from [85] (circles), [89] (triangles), and [10] (squares). The first and second numbers in each figure correspond to the photon energy E_γ (MeV) and the πN center-of-mass energy W (MeV), respectively.

$E_\gamma \simeq 700$–900 MeV were published by CBELSA/TAPS Collaboration [10]. By comparing with the new data we find that our chiral quark model calculation obviously underestimates the target asymmetry T in the higher energy region $E_\gamma > 700$ MeV, but the predicted tendency is in rough agreement with the data. In the low energy region $E_\gamma \simeq 280$–450 MeV, the data can be well described in the chiral quark model, though the data at forward and backward angles are still absent. In the energy region $E_\gamma \simeq 450$–660 MeV, our quark model results are obviously smaller than the data at the forward angle. To test our model, we expect that more precise measurements with large angle coverage can be carried out in the energy region $E_\gamma < 700$ MeV in the future. To clearly see contributions from different resonances, the energy dependent target asymmetries T at six angles $\theta_{\text{c.m.}} = 27^\circ, 50^\circ, 83^\circ, 100^\circ, 120^\circ, 145^\circ$ are shown in Fig. 10 as well. The data show that there is a dip structure at the angle $\theta_{\text{c.m.}} \simeq 80^\circ$–$100^\circ$ around the second resonance region $E_\gamma = 700$ MeV. This structure can be explained by the strong interference between $\Delta(1232)P_{33}$ and $N(1535)S_{11}$. Switching off the contributions of either $\Delta(1232)P_{33}$ or $N(1535)S_{11}$, no obvious dip structure around $E_\gamma = 700$ MeV can be found in the target asymmetry T. According to the chiral quark model predictions, the dip structure should be found at forward and backward angles as well. In the higher energy region $E_\gamma > 700$ MeV, it is found that many contributors, such as $\Delta(1232)P_{33}$, $N(1535)S_{11}$, $N(1650)S_{11}$, $N(1520)D_{13}$, $\Delta(1620)S_{31}$, $N(1720)P_{13}$, and the u-channel background have obvious effects on the target asymmetry T.

In brief, obvious roles of the $\Delta(1232)P_{33}$, $N(1535)S_{11}$, $N(1650)S_{11}$, $\Delta(1620)S_{31}$, $N(1520)D_{13}$, and $N(1720)P_{13}$ have been found in the $\gamma p \to \pi^0 p$ process. (i) $\Delta(1232)P_{33}$ not only plays a dominant role around the first resonance region, its strong contributions also extend up to the third resonance region, which can be obviously seen in the cross section, beam asymmetry, target asymmetry, and polarization of recoil protons. (ii) Both $N(1520)D_{13}$ and $N(1535)S_{11}$ play a dominant role around the second resonance region. They are the main contributors of the second bump structure in the energy dependent differential cross section and total cross section. Their strong effects on the polarization observables can be seen obviously as well. (iii) $N(1720)P_{13}$ might play a crucial role in the third resonance region. It might be responsible for the third bump structure in the energy dependent differential cross section and total cross section. However, no dominant role of $N(1720)P_{13}$ is found in the polarization observables. It should be pointed out that the evidence of $N(1720)P_{13}$ around the third resonance region should be further confirmed due to our poor descriptions of the polarization observables in the higher energy region. (iv) $\Delta(1620)S_{31}$ and $N(1650)S_{11}$ are crucial to give the correct shape of the differential cross sections in the second resonance region, although they do not contribute obvious structures in the cross sections. (v) Furthermore, the u- and t-channel backgrounds play crucial roles in the

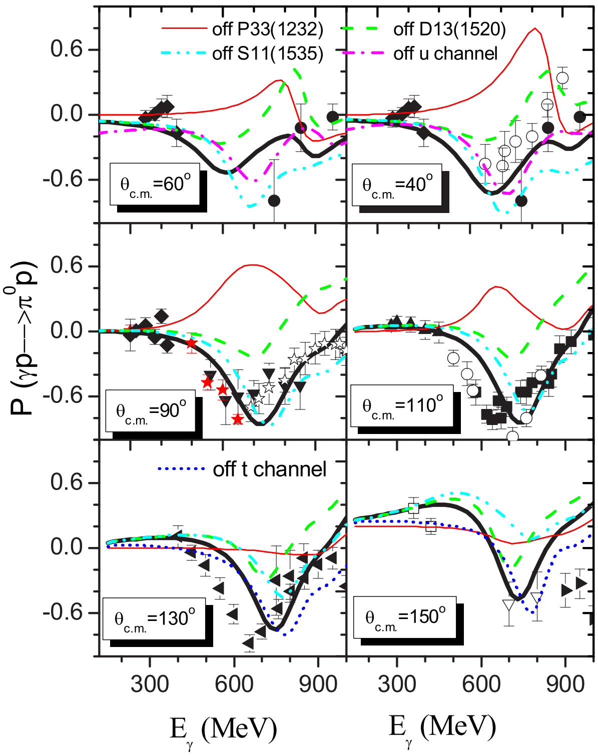

FIG. 8. (Color online) Photon energy dependent polarization of recoil protons for the $\gamma p \to \pi^0 p$ reaction. Data are taken from [90] (open circles), [91](solid circles), [92] (diamonds), [93] (solid down triangles), [94] (solid stars), [95] (open stars), [96] (solid squares), [85] (solid up triangles), [97] (solid left triangles), [98] (open down triangles), and [99] (solid right triangles). The results by switching off the contributions from various partial waves are indicated explicitly by different legends in the figure.

reaction as well. The u channel has a strong interference with the resonances, such as $\Delta(1232)P_{33}$, $N(1520)D_{13}$, and $N(1535)S_{11}$. Including the t-channel vector-meson exchange contribution, we find that the descriptions in the energy region $E_\gamma = 600$–900 MeV are improved obviously. (vi) No obvious contributions of the other resonances, such as $N(1700)D_{13}$, $\Delta(1700)D_{33}$, and $N(1680)F_{15}$, are found in the $\gamma p \to \pi^0 p$ process.

C. $\gamma n \to \pi^0 n$

The chiral quark model studies of $\gamma n \to \pi^0 n$ were carried out in Refs. [43,45,46] about twenty years ago. However, the model studies were limited in the first resonance region, because only a few scattered data were obtained from the old measurements in the early 1970s. Fortunately, obvious progress has been achieved in experiments in recent years. In 2009, some measurements of the beam asymmetries for the $\gamma n \to \pi^0 n$ process were obtained by the GRAAL experiment in the second and third resonances region [19]. In this energy region, recently the quasifree differential and total cross sections for this reaction were also measured by the Crystal Ball/TAPS experiment at MAMI [3]. Thus, these new measurements in the higher resonances region provide us a good opportunity to extend the chiral quark model to study these high-lying resonances.

The contributors of the s-channel intermediate states classified in the quark model with $n \leqslant 2$ have been listed in Table II. In the $n = 0$ shell, the dominant contribution to the reaction comes from the $\Delta(1232)P_{33}$, which has much larger CGLN amplitudes than the nucleon pole. In the $n = 1$ shell, three S-wave states $N(1535)S_{11}$, $N(1650)S_{11}$, and $\Delta(1620)S_{31}[70,{}^210]$ and four D-wave states $N(1520)D_{13}$, $N(1700)D_{13}$, $N(1675)D_{15}$, and $\Delta(1700)D_{33}$ contribute to the reaction. By comparing their CGLN amplitudes listed in Table II, we find that $N(1535)S_{11}$ and $N(1520)D_{13}$ play dominant roles in these S- and D-wave resonances. In the $n = 2$ shell, twelve P-wave resonance and seven F-wave resonances contribute to the reaction. Most of the P-wave and F-wave resonances in the $n = 2$ shell have comparable amplitudes. $N(1720)P_{13}$, $N(1900)P_{13}$, and $\Delta(1600)P_{33}$ have relatively larger CGLN amplitudes in the $n = 2$ shell P-wave resonances, while $N(1680)F_{15}$ and $\Delta(1905)F_{35}$ have relatively bigger CGLN amplitudes among the $n = 2$ shell F-wave resonances.

In this work, we have carried out a chiral quark model study of the $\gamma n \to \pi^0 n$ reaction up to the second and third resonances region. In the SU(6)⊗O(3) symmetry limit, the parameters from the u- and t-channel backgrounds and the Δ resonances $\Delta(1232)P_{33}$ and $\Delta(1620)S_{31}$ for the $\pi^0 n$ channel should be the same as those for the $\pi^0 p$ channel, which have been well determined by the γp data. Thus, in the $\gamma n \to \pi^0 n$ reaction these parameters are taken to have the same values as in the $\gamma p \to \pi^0 p$ process. The other strength parameters, C_R, for the main resonances $N(1535)S_{11}$, $N(1650)S_{11}$, $N(1520)D_{13}$, and $N(1720)P_{13}$ for the γn reaction cannot be well constrained by the γp data for their different photocouplings; thus, we determine them by fitting the 36 γn data points of total cross section around the second resonance energy region $1.30 \leqslant W \leqslant 1.72$ GeV recently measured at MAMI [3]. The χ^2 datum point is about $\chi^2/N_{\rm data} = 2.8$. Our results compared with the data are shown in Figs 11–16.

The differential cross sections compared with the data are shown in Fig. 11. In the energy region what we consider, only a few data can be obtained. Fortunately, the abundant data for the $\gamma p \to \pi^0 p$ process help us well constrain some important model parameters, as we pointed out above. From Fig. 11, one can see that the data of the $\gamma n \to \pi^0 n$ reaction are reasonably reproduced. To clearly see the contributions from different partial waves, we plot the energy dependent differential cross sections in Fig. 12 as well. Our results obviously show three bump structures in the forward angle region. It is found that the resonances $\Delta(1232)P_{33}$, $N(1535)S_{11}$, $N(1520)D_{13}$, and $N(1720)P_{13}$ play crucial roles in the $\gamma n \to \pi^0 n$ reaction. The $\Delta(1232)P_{33}$ resonance is responsible for the first bump structure around $E_\gamma \simeq 300$ MeV. Both $N(1535)S_{11}$ and $N(1520)D_{13}$ are the main contributors to the second bump around $E_\gamma \simeq 700$ MeV. The $N(1720)P_{13}$ resonance is most likely responsible for the third bump around $E_\gamma \simeq 1000$ MeV.

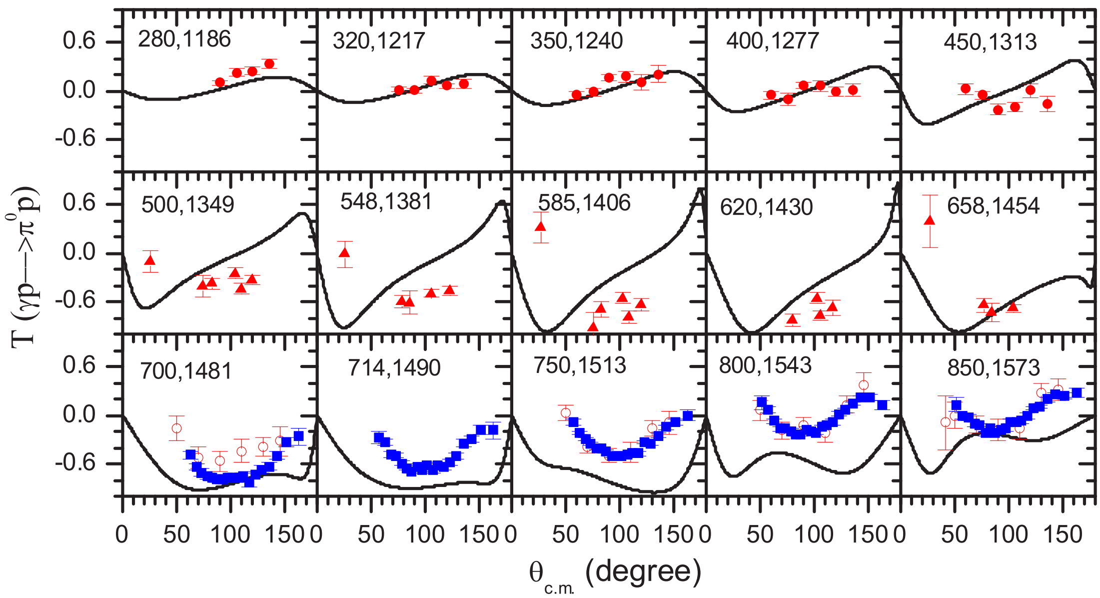

FIG. 9. (Color online) Target asymmetry of the $\gamma p \to \pi^0 p$ reaction as a function of scattering angle. The data are taken from [85] (solid circles), [100] (solid triangles), [101] (open circles), and [10] (solid squares). The first and second numbers in each figure correspond to the photon energy E_γ (MeV) and the πN center-of-mass energy W (MeV), respectively.

The total cross sections compared with the data are shown in Fig. 13. Obvious roles of $\Delta(1232)P_{33}$, $N(1535)S_{11}$, and $N(1720)P_{13}$ in the $\gamma n \to \pi^0 n$ reaction can be found in the total cross section as well. Recently, the total cross section was measured by the Crystal Ball/TAPS experiment at MAMI [3]. There are two obvious bump structures in the cross section in the second and third resonances region (see Fig. 13). The bump structure around the second resonance region receives approximately equal contributions from $N(1535)S_{11}$ and $N(1520)D_{13}$, while the bump structure around the third resonance region might be due to the contributions of $N(1720)P_{13}$. There are no measurements of the total cross section in the first resonance region. In this energy region, we predict that the ratio of total cross section between the $\pi^0 n$ channel and the $\pi^0 p$ channel σ_n/σ_p is around 1 (see Fig. 14).

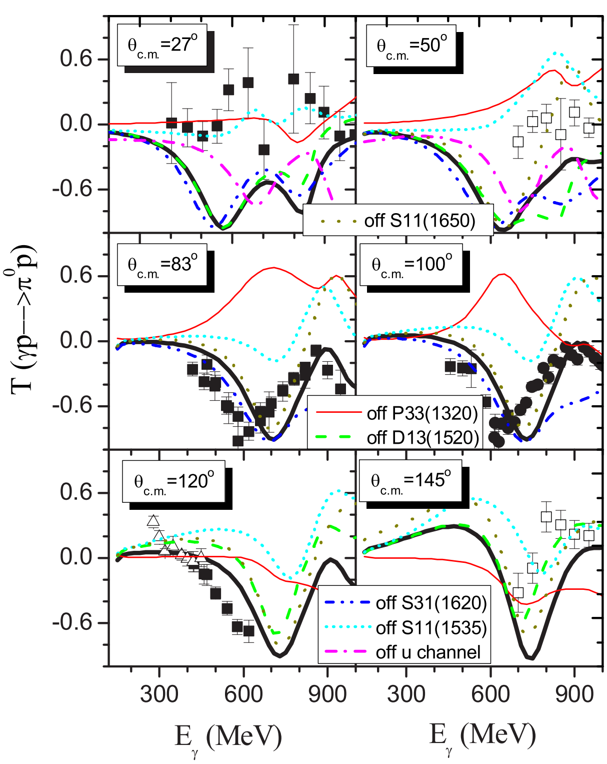

FIG. 10. (Color online) Photon energy dependent target asymmetry of the $\gamma p \to \pi^0 p$ reaction. The data are taken from [100] (solid squares), [101] (open squares), [102] (solid circles), and [85] (open triangles). The results by switching off the contributions from various partial waves are indicated explicitly by different legends in the figure.

Furthermore, by analyzing the data of differential and total cross sections, we find that $\Delta(1620)S_{31}$ and $N(1650)S_{11}$ play obvious roles around their mass threshold. If we switch off them, the cross sections around their mass threshold are overestimated significantly. It should be mentioned that the role of $N(1650)S_{11}$ should be confirmed by more accurate data in the future, which will be further discussed in Sec. III D. Finally, it should be pointed out that the backgrounds play a crucial role in the reaction. The u-channel background has strong destructive interference with $\Delta(1232)P_{33}$, $N(1535)S_{11}$, $N(1520)D_{13}$, and $N(1720)P_{13}$. Including the t-channel vector-meson exchange contribution, we find that the descriptions of the cross sections in the energy region $E_\gamma = 600$–900 MeV are improved significantly.

The polarization observations for the $\gamma n \to \pi^0 n$ reaction are very sparse. In 2009, the beam asymmetry Σ in the second and third resonances region was measured by the GRAAL Collaboration for the first time [19]. Our chiral quark model results are shown in Fig. 15. From the figure, it is seen that the model results are in rough agreement with the data. Our results are notably smaller than the data at intermediate angles. To clearly see the contributions from

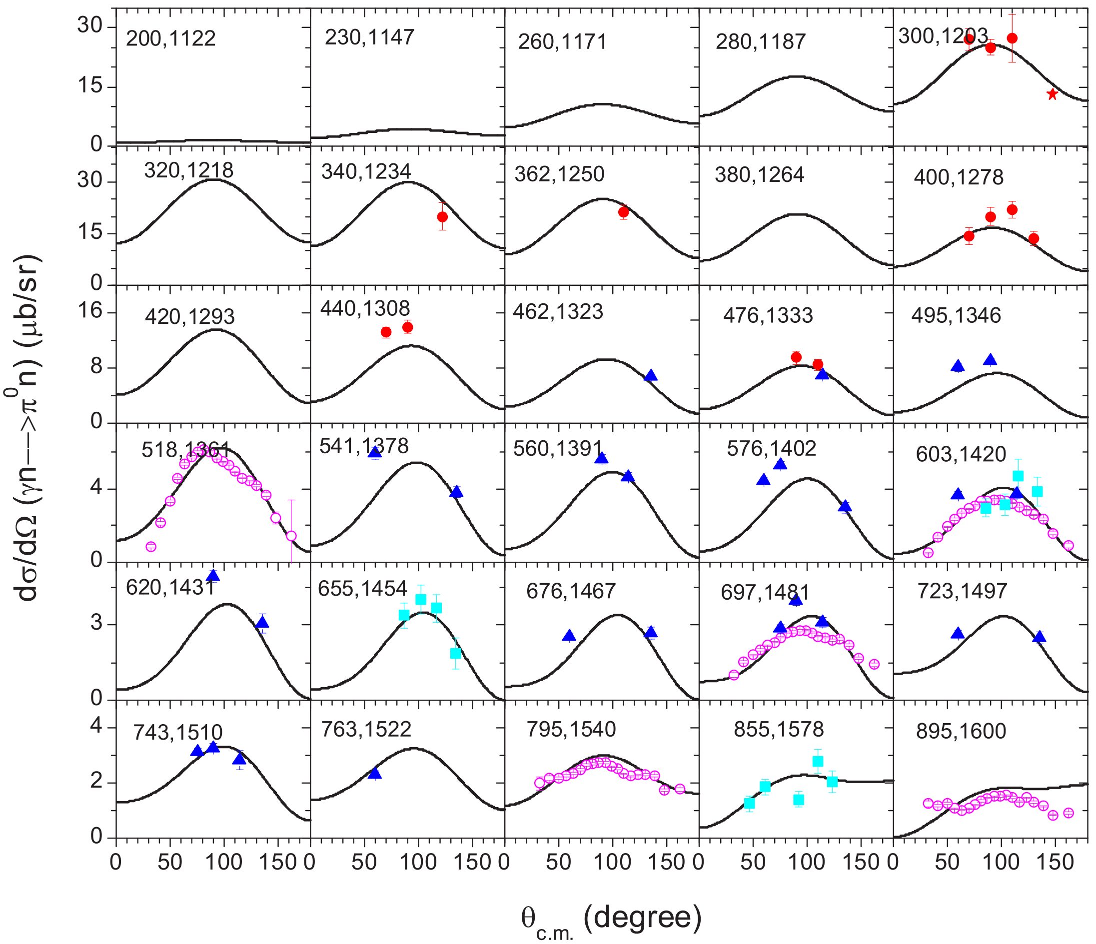

FIG. 11. (Color online) Differential cross sections of the $\gamma n \to \pi^0 n$ reaction as a function of scattering angle. Data are taken from [3] (open circles), [103] (solid circles), [104] (solid squares), and [105] (solid triangles). The first and second numbers in each figure correspond to the photon energy E_γ (MeV) and the πN center-of-mass energy W (MeV), respectively.

different partial waves, the energy dependent beam asymmetries Σ at six angles $\theta_{\text{c.m.}} = 20^\circ, 52^\circ, 91^\circ, 123^\circ, 144^\circ, 163^\circ$ are shown in Fig. 16 as well. From the figure, one can find that, below the photon energy $E_\gamma \simeq 500$ MeV, the beam asymmetry is sensitive to $\Delta(1232)P_{33}$ and the u-channel background. By turning off one of them, the beam asymmetry changes drastically in this energy region. Similarly, we can obviously find that around the second resonance region, i.e., $E_\gamma \sim 700$ MeV, the $N(1535)S_{11}$, $N(1650)S_{11}$, $N(1520)D_{13}$, $\Delta(1232)P_{33}$, $\Delta(1620)S_{31}$, and the u-channel background have strong effects on the beam asymmetry. Up to the second resonance region, the higher partial wave states, such as $N(1720)P_{13}$, begin to contribute to beam asymmetry. Many resonances together with the backgrounds have approximately equal contributions to the beam asymmetry, leading to a very complicated description of the data.

As a whole, a reasonable chiral quark model description of the $\gamma n \to \pi^0 n$ reaction is obtained from the pion production threshold up to the second resonance region. Obvious evidences of the $\Delta(1232)P_{33}$, $N(1535)S_{11}$, $N(1520)D_{13}$, and $N(1720)P_{13}$ are also found in the $\gamma n \to \pi^0 n$ reaction. (i) The ground state $\Delta(1232)P_{33}$, the S-wave state $N(1535)S_{11}$ together with the D-wave state $N(1520)D_{13}$, and the P-wave state $N(1720)P_{13}$ are responsible for the first, second, and third bump structures in the cross sections, respectively. (ii) Furthermore, another two S-wave states $\Delta(1620)S_{31}$ and $N(1650)S_{11}$ have obvious effects on the differential cross section around their mass threshold, although they do not give any structure in the cross sections. It should be pointed out that the role of $N(1650)S_{11}$ should be further confirmed in future experiments. (iii) The backgrounds play a crucial role in the reaction. The u channel background has a strong constructive interference with the s-channel resonances $\Delta(1232)P_{33}$, $N(1535)S_{11}$, and $N(1520)D_{13}$. By including the t-channel vector-meson exchange contribution, we find that the descriptions in the energy region $E_\gamma = 600$–900 MeV are slightly improved. (vi) No obvious evidence of the other resonances, such as $N(1700)D_{13}$, $N(1675)D_{15}$, $\Delta(1700)D_{33}$, and $N(1680)F_{15}$, is found in the $\gamma n \to \pi^0 n$ process.

D. Helicity amplitudes

The accurate data for the $\gamma n \to \pi^0 n$ and $\gamma p \to \pi^0 p$ processes provide us a good platform to extract the helicity amplitudes of the dominant resonances in these reactions. Theoretically, the helicity amplitudes A_λ for a baryon

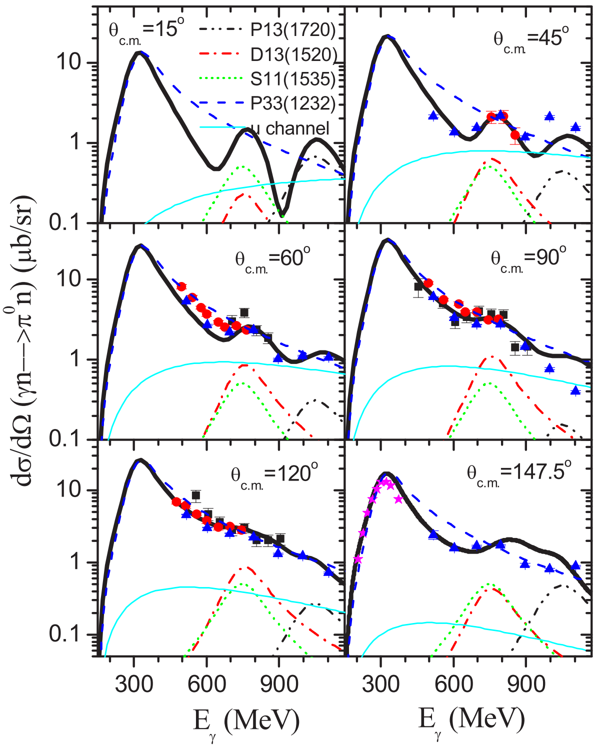

FIG. 12. (Color online) Photon energy dependent differential cross sections of the $\gamma n \to \pi^0 n$ reaction. Data are taken from [3] (solid triangles), [106] (solid stars), [104] (solid squares), and [105] (solid circles). The partial cross sections for $\Delta(1232)P_{33}$, $N(1535)S_{11}$, $N(1520)D_{13}$, and $N(1720)P_{13}$ are indicated explicitly by different legends in the figure.

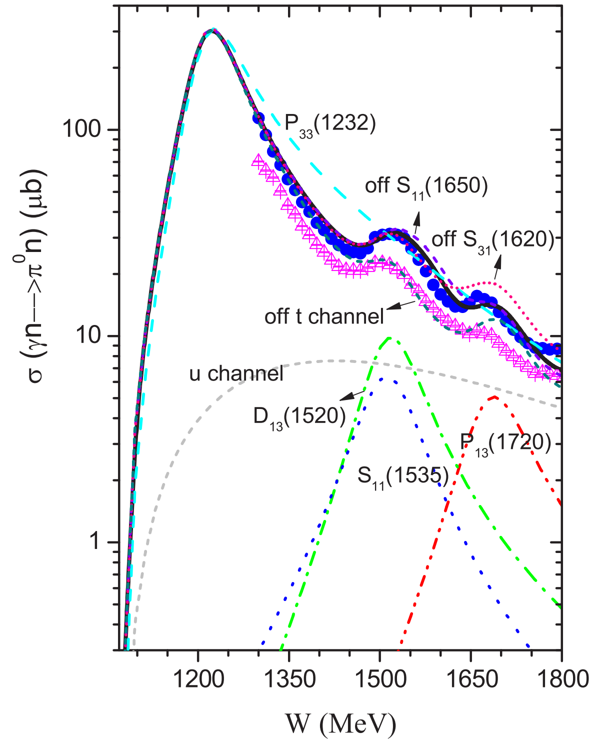

FIG. 13. (Color online) Total cross section as a function of the c.m. energy W for the $\gamma n \to \pi^0 n$ reaction. Data are taken from [3]. The results by switching off the contributions from $N(1650)S_{11}$, $\Delta(1620)S_{31}$, and t channel and the partial cross sections for $\Delta(1232)P_{33}$, $N(1535)S_{11}$, $N(1520)D_{13}$, $N(1720)P_{13}$, and u channel are indicated explicitly by different legends in the figure.

resonance N^* photoexcitation on a nucleon are defined by

$$A_\lambda = \sqrt{2\pi/k}\langle N^*; J_z = \lambda | H_e | N; J_z = \lambda - 1\rangle, \quad (31)$$

where $\lambda = 1/2$ and $3/2$. As we know, the helicity amplitudes of a resonance are related to the transition amplitudes of the photoproduction reactions. Thus, we can extract the helicity amplitudes from the neutral pion photoproduction processes by the relation

$$A^{n,p}_{1/2,3/2} = \sqrt{\frac{|\mathbf{q}| M_R \Gamma_R}{|\mathbf{k}| M_N b_{\pi^0 N}}}\, \xi^{n,p}_{1/2,3/2}, \quad (32)$$

where $b_{\pi^0 N} \equiv \Gamma_{\pi^0 N}/\Gamma_R$ is the branching ratio of the resonance. The quantity ξ for different resonances can be analytically expressed from their CGLN amplitudes. We have given the expressions of the ξ for several low-lying nucleon and Δ resonances in Table VI. We estimate the helicity amplitudes for these main contributing resonances: $\Delta(1232)P_{33}$, $\Delta(1620)S_{31}$, $N(1535)S_{11}$, $N(1650)S_{11}$, $N(1520)D_{13}$, and $N(1720)P_{13}$. The branching ratios $b_{\pi N}$ for $N(1720)P_{13}$ are adopted from our quark model prediction, and the branching ratios for other resonances are taken from PDG14 [34] (see Table VII). Our extracted helicity amplitudes are listed in Table VIII. As a comparison, in the same table we also show our previous solution extracted from the η photoproduction processes [38], the recent analyses of the γN data from SAID [23–25], Kent [27], and BnGa [20,22], the average values from PDG14 [34], and the theoretical predictions from different quark models [107,108].

From Table VIII, it is found that the helicity amplitudes of $\Delta(1232)P_{33}$ extracted in present work are in good agreement with the values from PDG14 [34] and other partial wave analysis groups [20,22–25,27,109].

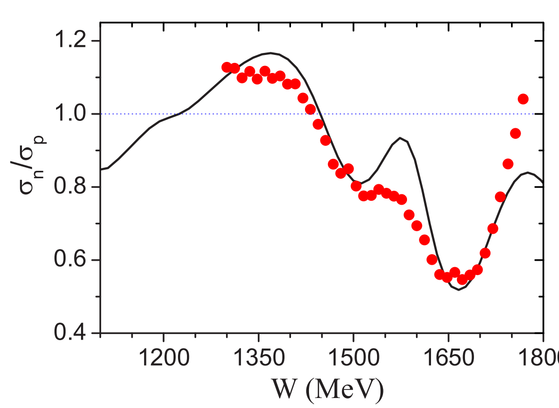

FIG. 14. (Color online) Cross section ratio σ_n/σ_p between the reactions $\gamma n \to \pi^0 n$ and $\gamma p \to \pi^0 p$ as a function of the center-of-mass energy W. Data are taken from Ref. [3].

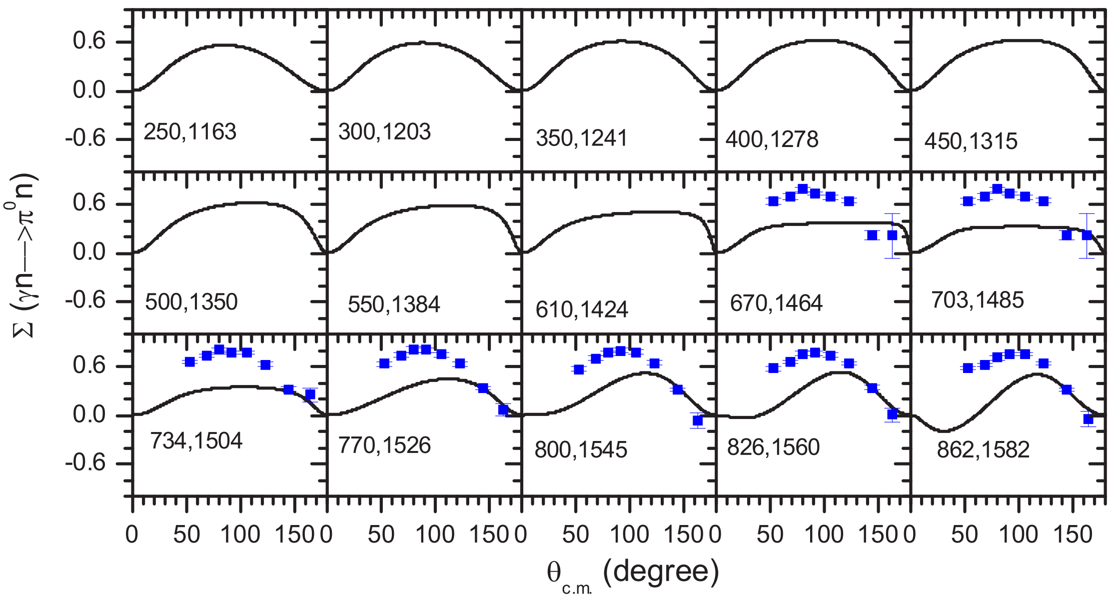

FIG. 15. (Color online) Beam asymmetry of the $\gamma n \to \pi^0 n$ reaction as a function of scattering angle. Data are taken from [19]. The first and second numbers in each figure correspond to the photon energy E_γ (MeV) and the πN center-of-mass energy W (MeV), respectively.

The $A^p_{1/2}$ and $A^n_{1/2}$ of $N(1535)S_{11}$ extracted in this work are compatible with the PDG average values and the latest analysis of the γN data from SAID [23–25]. It should be pointed out that with the same model we found a smaller γp coupling $A^p_{1/2} \simeq 60 \times 10^{-3}$ GeV$^{-1/2}$ for $N(1535)S_{11}$ by analysis of the $\gamma p \to \eta p$ process [38], and similar solution was also obtained in [52,110]. The reason for the different γp couplings for $N(1535)S_{11}$ in the $\pi^0 p$ and ηp channels should be clarified in future studies.

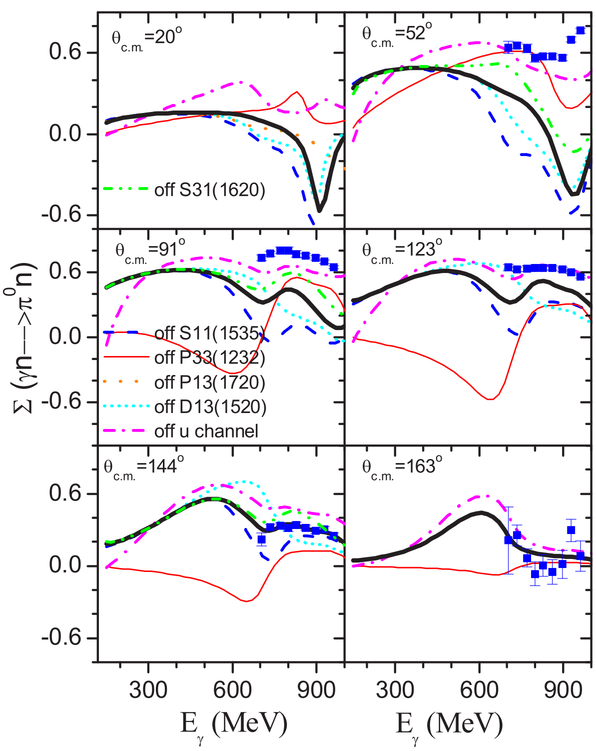

FIG. 16. (Color online) Photon energy dependent beam asymmetry of the $\gamma n \to \pi^0 n$ reaction. Data are taken from [19]. The results by switching off the contributions from various partial waves are indicated explicitly by different legends in the figure.

All the partial wave analysis groups have extracted similar γp coupling $A^p_{1/2}$ for $N(1650)S_{11}$ from the data, which is also consistent with the theoretical predictions in quark models [107,108]. However, contradictory solutions for the γn coupling $A^n_{1/2}$ of $N(1650)S_{11}$ are obtained by different groups. Our previous analysis of the $\gamma n \to \eta n$ reaction indicates a positive helicity coupling $A^n_{1/2} \simeq 24 \times 10^{-3}$ GeV$^{-1/2}$ for $N(1650)S_{11}$ [38], which is supported by the latest analysis of the same reaction from the BnGa [22,39] and Kent [27] groups. However, in present work by analyzing the recent the final-state-interaction (FSI) corrected data of the $\gamma n \to \pi^0 n$ reaction from the A2 Collaboration [3], a negative helicity coupling $A^n_{1/2} \simeq -18 \times 10^{-3}$ GeV$^{-1/2}$ is obtained, which is compatible with the values from PDG14 [34] and the recent SAID analysis [23–25]. Contradictory results for the γn coupling $A^n_{1/2}$ of $N(1650)S_{11}$ obtained from two different reactions with the same model indicate that the $N(1650)S_{11}$ state found in the $\gamma n \to \pi^0 n$ is possibly not the same state found in the $\gamma n \to \eta n$ if the data are accurate enough. It should be noted that the FSI is a rather rough correction that assumes identical effects on the proton and the neutron, which certainly does not have to be the case [3]. Thus, considering that the data from the A2 Collaboration might bear large uncertainties in the second resonance region, with a small positive helicity amplitude, $A^n_{1/2} \simeq 20 \times 10^{-3}$ GeV$^{-1/2}$ for $N(1650)S_{11}$, we predict the differential and total cross sections around the second resonance region (see Fig. 17). If $N(1650)S_{11}$ has a positive helicity amplitude, it is found that (i) the differential cross section and the total cross section around the second resonance region should be significantly larger than the present data, and (ii) $N(1650)S_{11}$ has obviously

TABLE VI. The expressions of ξ in Eq. (32) for various resonances. Here we have defined $\mathcal{K}\equiv\sqrt{\frac{\alpha_e\alpha_\pi(E_f+M_N)\pi}{2M_R^2M_N}\frac{1}{\Gamma_R}}$, $\mathcal{A}\equiv[\frac{2\omega_\gamma}{m_q}-\frac{2q^2}{3\alpha^2}(1+\frac{\omega_\pi}{E_f+M_N})]e^{-\frac{k^2+q^2}{6\alpha^2}}$, $\mathcal{B}\equiv\frac{2q^2}{3\alpha^2}(1+\frac{\omega_\pi}{E_f+M_N})e^{-\frac{k^2+q^2}{6\alpha^2}}$, and $\mathcal{D}\equiv[\frac{2\omega_\gamma}{m_q}-\frac{2q^2}{5\alpha^2}(1+\frac{\omega_\pi}{E_f+M_N})]e^{-\frac{k^2+q^2}{6\alpha^2}}$.

$\Delta(1232)P_{33}$	$\xi_{1/2}$	$-\mathcal{K}\sqrt{\frac{1}{2}}\frac{4\omega_\gamma}{9m_q}(1+\frac{\omega_\pi}{E_f+M_N})\lvert\mathbf{q}\rvert C_{P_{33}(1232)}$
	$\xi_{3/2}$	$-\mathcal{K}\sqrt{\frac{3}{2}}\frac{4\omega_\gamma}{9m_q}(1+\frac{\omega_\pi}{E_f+M_N})\lvert\mathbf{q}\rvert C_{P_{33}(1232)}$
$\Delta(1620)S_{31}$	$\xi_{1/2}$	$\mathcal{K}\frac{\omega_\gamma}{18}(1-\frac{\omega_\gamma}{6m_q})\mathcal{A}C_{S_{31}(1620)}$
$N(1535)S_{11}$	$\xi^p_{1/2}$	$\mathcal{K}\frac{\omega_\gamma}{9}(1+\frac{\omega_\gamma}{2m_q})\mathcal{A}C^{[70,^28]}_{S_{11}(1535)}$
	$\xi^n_{1/2}$	$-\mathcal{K}\frac{\omega_\gamma}{9}[(1+\frac{\omega_\gamma}{6m_q})+\frac{\tan\theta_S\omega_\gamma}{6m_q}]\mathcal{A}C^{[70,^28]}_{S_{11}(1535)}$
$N(1650)S_{11}$	$\xi^p_{1/2}$	$\mathcal{K}\frac{\omega_\gamma}{9}(1+\frac{\omega_\gamma}{2m_q})\mathcal{A}C^{[70,^28]}_{S_{11}(1650)}$
	$\xi^n_{1/2}$	$-\mathcal{K}\frac{\omega_\gamma}{9}[(1+\frac{\omega_\gamma}{6m_q})-\frac{\cot\theta_S\omega_\gamma}{6m_q}]\mathcal{A}C^{[70,^28]}_{S_{11}(1650)}$
$N(1520)D_{13}$	$\xi^p_{1/2}$	$\mathcal{K}\frac{\omega_\gamma}{9\sqrt{2}}(1-\frac{\omega_\gamma}{m_q})\mathcal{B}C^{[70,^28]}_{D_{13}(1520)}$
	$\xi^p_{3/2}$	$\mathcal{K}\sqrt{\frac{3}{2}}\frac{\omega_\gamma}{9}\mathcal{B}C^{[70,^28]}_{D_{13}(1520)}$
	$\xi^n_{1/2}$	$-\mathcal{K}\frac{\omega_\gamma}{9\sqrt{2}}[(1-\frac{\omega_\gamma}{3m_q})-\frac{\tan\theta_D\omega_\gamma}{3\sqrt{10}m_q}]\mathcal{B}C^{[70,^28]}_{D_{13}(1520)}$
	$\xi^n_{3/2}$	$-\sqrt{\frac{3}{2}}\mathcal{K}\frac{\omega_\gamma}{9}[1-\frac{\tan\theta_D\omega_\gamma}{\sqrt{10}m_q}]\mathcal{B}C^{[70,^28]}_{D_{13}(1520)}$
$N(1700)D_{13}$	$\xi^n_{1/2}$	$-\frac{\omega_\gamma}{9\sqrt{2}}\mathcal{K}[(1-\frac{\omega_\gamma}{3m_q})+\frac{\cot\theta_D\omega_\gamma}{3\sqrt{10}m_q}]\mathcal{B}C^{[70,^28]}_{D_{13}(1700)}$
	$\xi^n_{3/2}$	$-\sqrt{\frac{3}{2}}\mathcal{K}\frac{\omega_\gamma}{9}[1+\frac{\cot\theta_D\omega_\gamma}{\sqrt{10}m_q}]\mathcal{B}C^{[70,^28]}_{D_{13}(1700)}$
	$\xi^p_{1/2}$	$\mathcal{K}\sqrt{\frac{1}{2}}\frac{\omega_\gamma}{9}(1-\frac{\omega_\gamma}{m_q})\mathcal{B}C^{[70,^28]}_{D_{13}(1700)}$
	$\xi^p_{3/2}$	$\mathcal{K}\sqrt{\frac{3}{2}}\frac{\omega_\gamma}{9}\mathcal{B}C^{[70,^28]}_{D_{13}(1700)}$
$N(1675)D_{15}$	$\xi^n_{1/2}$	$-\mathcal{K}\frac{\omega_\gamma^2}{40m_q}\mathcal{B}C_{D_{15}(1675)}$
	$\xi^n_{3/2}$	$-\mathcal{K}\frac{\omega_\gamma^2}{20\sqrt{2}m_q}\mathcal{B}C_{D_{15}(1675)}$
$N(1720)P_{13}$	$\xi^p_{1/2}$	$\mathcal{K}\sqrt{\frac{1}{2}\frac{5}{108}\frac{\omega_\gamma^2}{\alpha^2}}(1+\frac{k}{3m_q})\mathcal{D}\lvert\mathbf{q}\rvert C^p_{P_{13}(1720)}$
	$\xi^p_{3/2}$	$-\mathcal{K}\sqrt{\frac{1}{6}\frac{5}{108}\frac{\omega_\gamma^2}{\alpha^2}}\mathcal{D}\lvert\mathbf{q}\rvert C^p_{P_{13}(1720)}$
	$\xi^n_{1/2}$	$-\mathcal{K}\sqrt{\frac{1}{2}\frac{5}{108}\frac{\omega_\gamma^2}{\alpha^2}}\frac{2k}{27m_q}\mathcal{D}\lvert\mathbf{q}\rvert C^n_{P_{13}(1720)}$
	$\xi^n_{3/2}$	0

constructive interference with $N(1535)S_{11}$ and $N(1520)D_{13}$, which can be tested in future experiments. It was pointed out in Ref. [111] that the positive $A^n_{1/2}$ would imply $N(1650)S_{11}$ should have a large $s\bar{s}$ component in its wave function. To clarify the sign problem of the γn coupling for $N(1650)S_{11}$, more accurate data are needed.

We find a large helicity amplitude for $\Delta(1620)S_{31}$, which is about a factor 2 larger than the PDG average value [34], and 30% larger than the recent results from the BnGa [20,22] and

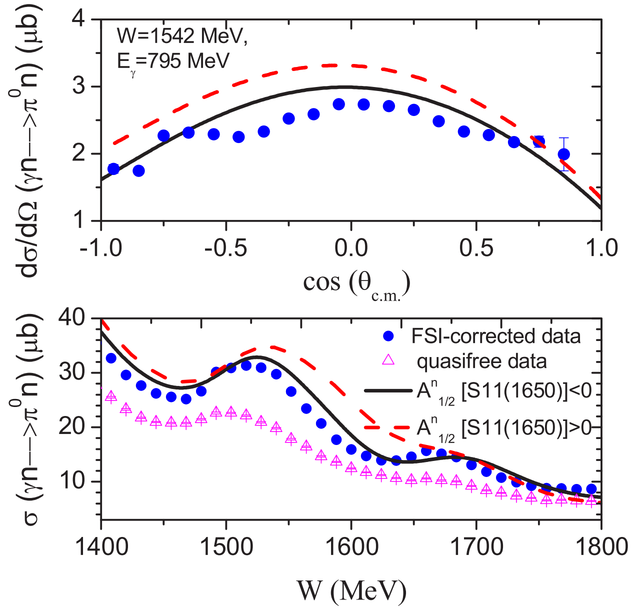

FIG. 17. (Color online) Effects of $N(1650)S_{11}$ on the differential cross sections and the total cross section around its mass threshold. Data are taken from Ref. [3]. The solid and dashed curves are for the results with negative and positive γn couplings for $N(1650)S_{11}$, respectively.

SAID [25] groups. However, we find that our result is very close to the theoretical predictions in quark models [107,108].

In our previous work [38], we gave our estimations of the helicity amplitudes for $N(1520)D_{13}$ by the analysis of the η photoproduction data. However, the large uncertainties of the branching ratio $b_{\eta N}$ lead to a weak conclusion of these helicity amplitudes. In this work, the accurate branching ratio $b_{\pi N}$ should let us extract the helicity amplitudes for $N(1520)D_{13}$ more reliably. It is found that the $A^p_{1/2}$ extracted by us is in good agreement with the results from the SAID group [25] and the PDG average value [34]. However, the $A^p_{3/2}$ extracted in present work are about 30% smaller than the PDG average value [34] and the results from other groups. It should be mentioned that recently the CBELSA/TAPS Collaboration also found a small helicity amplitude $A^p_{3/2}\simeq 118\times10^{-3}$ GeV$^{-1/2}$ from an energy-independent multipole analysis based on new polarization data on photoproduction of neutral pions [10]. The γn couplings for the $N(1520)D_{13}$ extracted in this work are compatible with the PDG values within 30% uncertainties. Our results are slightly smaller than the results from other partial wave analysis groups.

For $N(1720)P_{13}$, we note that the absolute values of the $A^p_{1/2}$ and $A^p_{3/2}$ extracted by us are compatible with the results from the BnGa [20,22] and Kent [27] groups. However, their solutions have opposite signs to our results. It is interesting to find that our results are consistent with the quark model

TABLE VII. Branching ratio $b_{\pi N}$ of the resonances used in the calculation.

Resonance	$\Delta(1232)P_{33}$	$\Delta(1620)S_{31}$	$N(1535)S_{11}$	$N(1650)S_{11}$	$N(1520)D_{13}$	$N(1720)P_{13}$
$b_{\pi N}$	1.0	20–30 %	35–55 %	50–90 %	55–65 %	60–90 %

TABLE VIII. Extracted helicity amplitudes for the main nucleon and $\Delta(1232)$ resonances from the neutral pion photoproduction reactions (in units of 10^{-3} GeV$^{-1/2}$).

Resonance	Helicity	This work	ZZ11[38]	PDG14 [34]	Kent12 [27]	BnGa [20,22]	SAID12 [23,24]	SAID11[25]	ZF [107]	C92 [108]
$\Delta(1232)P_{33}$	$A_{1/2}$	-133		-135 ± 6	-137 ± 1	-136 ± 5	-139 ± 2	-138 ± 3	-94	-108
	$A_{3/2}$	-230		-255 ± 5	-251 ± 1	-267 ± 8	-262 ± 3	-259 ± 5	-162	-186
$N(1535)S_{11}$	$A^p_{1/2}$	137 ± 15	60 ± 5	115 ± 15	59 ± 3	90 ± 15	128 ± 4	99 ± 2	142	76
	$A^n_{1/2}$	-77 ± 9	-68 ± 5	-75 ± 20	-49 ± 3	-93 ± 11	-58 ± 6	-60 ± 3	-77	-63
$N(1650)S_{11}$	$A^p_{1/2}$	61 ± 9	41 ± 13	45 ± 10	30 ± 3	60 ± 20	55 ± 30	65 ± 25	78	54
	$A^n_{1/2}$	-18 ± 3	24 ± 7	-50 ± 20	11 ± 2	25 ± 20	-40 ± 10	-26 ± 8	-47	-35
$\Delta(1620)S_{31}$	$A_{1/2}$	80 ± 8		40 ± 15	-3 ± 3	63 ± 12	29 ± 3	64 ± 2	72	81
$N(1520)D_{13}$	$A^p_{1/2}$	-17 ± 1	-32 ± 7	-20 ± 5	-34 ± 1	-32 ± 6	-19 ± 2	-16 ± 2	-47	-15
	$A^p_{3/2}$	109 ± 5	113 ± 23	140 ± 10	127 ± 3	138 ± 8	141 ± 2	156 ± 2	117	134
	$A^n_{1/2}$	-30 ± 1	-40 ± 8	-50 ± 10	-38 ± 3	-49 ± 8	-46 ± 6	-47 ± 2	-75	-38
	$A^n_{3/2}$	-90 ± 4	-126 ± 26	-115 ± 10	-101 ± 4	-113 ± 12	-115 ± 5	-125 ± 2	-127	-114
$N(1720)P_{13}$	$A^p_{1/2}$	-89 ± 9		100 ± 20	57 ± 3	130 ± 50	95 ± 2	99 ± 3	-68	-11
	$A^p_{3/2}$	34 ± 4			-19 ± 2	100 ± 50	-48 ± 2	-43 ± 2	53	-31
	$A^n_{1/2}$	18 ± 2			-2 ± 1	-80 ± 50		-21 ± 4	-4	4
	$A^n_{3/2}$	0			-1 ± 2	-140 ± 65		-38 ± 7	-33	11

predictions by Li and Close [107] and the partial wave analysis of the $\gamma n \to \eta n$ reaction from Giessen group [110]. Knowledge about the γn couplings, $A^n_{1/2}$ and $A^n_{3/2}$, for the $N(1720)P_{13}$ is very poor, and different groups have given very different predictions. In the SU(6)⊗O(3) symmetry limit, we predict the $A^n_{3/2}$ should be zero, which is compatible with the analysis of the Kent group [27]. More studies are needed to clarify these puzzles about $N(1720)P_{13}$.

IV. SUMMARY

In this work, we have studied neutral pion photoproduction on nucleons within a chiral quark model. We have achieved reasonable descriptions of the data from the pion production threshold up to the second resonance region.

The roles of the low-lying resonances in the reactions were carefully analyzed. We found that (i) $\Delta(1232)P_{33}$, $N(1535)S_{11}$, $N(1520)D_{13}$, and $N(1720)P_{13}$ play crucial roles in both $\gamma p \to \pi^0 p$ and $\gamma n \to \pi^0 n$ reactions. The $\Delta(1232)P_{33}$ resonance not only plays a dominant role around the first resonance region, but also contributes up to the third resonance region. Both $N(1535)S_{11}$ and $N(1520)D_{13}$ paly crucial roles around the second resonance region. The second bump structure around $E_\gamma = 700$ MeV in the cross section receives approximately equal contributions from these two resonances. $N(1720)P_{13}$ might play a crucial role in the third resonance region. It might be responsible for the third bump structure in cross section, which should be further investigated due to our relatively poor descriptions of the polarization observables in this energy region. (ii) Furthermore, obvious evidence of $N(1650)S_{11}$ and $\Delta(1620)S_{31}$ is also found in the reactions. They notably affect the cross sections and the polarization observables from the second resonance region to the third resonance region. (iii) The u- and t-channel backgrounds play a crucial role in the reaction as well. The u channel has strong interference with the resonances, such as $\Delta(1232)P_{33}$, $N(1535)S_{11}$, and $N(1520)D_{13}$. By including the t-channel vector-meson exchange contribution, the descriptions of the data in the energy region $E_\gamma = 600$–900 MeV are improved notably. (iv) No obvious evidence of the other resonances, e.g., $N(1700)D_{13}$, $N(1675)D_{15}$, $\Delta(1700)D_{33}$, and $N(1680)F_{15}$, was found in the reactions.

Furthermore, the helicity couplings for the main resonances, $\Delta(1232)P_{33}$, $N(1535)S_{11}$, $N(1520)D_{13}$, $N(1720)P_{13}$, $N(1650)S_{11}$, and $\Delta(1620)S_{31}$, were extracted from the reactions. We found that (i) uur extracted helicity amplitudes of $\Delta(1232)P_{33}$ and $N(1535)S_{11}$ are in good agreement with the PDG average values and the results of other groups. (ii) The γp coupling for $N(1650)S_{11}$ extracted by us is in good agreement with the results from SAID [23–25] and BnGa [20,22]. However, properties of the γn coupling for $N(1650)S_{11}$ are still controversial. Our analysis of the recent data of the $\gamma n \to \pi^0 n$ reaction indicates a small negative γn coupling for $N(1650)S_{11}$. Its sign is opposite to that of other analyses of the $\gamma n \to \eta n$ data [22,38,39]. (iii) We obtain a large helicity coupling for $\Delta(1620)S_{31}$, but it is very close to the recent analysis from the BnGa group [20,22]. (iv) We give smaller helicity couplings for $N(1520)D_{13}$, which are compatible with the PDG values at the 30% level. (v) The helicity couplings $A^p_{1/2}$ and $A^p_{3/2}$ for $N(1720)P_{13}$ extracted by us are consistent with the quark model predictions by Li and Close [107,108] and the analysis of the Giessen group [110]. We find a small positive helicity coupling $A^n_{1/2}$ for $N(1720)P_{13}$, and the $A^n_{3/2}$ should be zero in the SU(6)⊗O(3) symmetry limit.

Finally, it should be pointed out that (i) the width of $N(1720)P_{13}$ extracted by us is notably narrower than the estimated values from the PDG; however, our result is in good agreement with those extracted from the $\pi^- p \to K^0\Lambda$ reaction by Saxon *et al.* [74]. To confirm the properties of $N(1720)P_{13}$, a study of the $\pi^- p \to K^0\Lambda$ reaction is needed. (ii) Furthermore, a more realistic correction of the FSI for neutral pion photoproduction on quasifree neutrons hopefully will be obtained in future. Then the sign problem of the γn coupling $A^n_{1/2}$ of $N(1650)S_{11}$ could be clarified in the $\gamma n \to \pi^0 n$ reaction, which seems to be crucial to uncover the puzzle of the narrow structure around $W = 1.68$ GeV observed in the excitation function of η production off quasifree neutrons. If the γn coupling $A^n_{1/2}$ of $N(1650)S_{11}$ is negative, then the narrow structure in the $\gamma n \to \eta n$ reaction would no longer be explained by the interference effects between $N(1535)S_{11}$ and $N(1650)S_{11}$.

ACKNOWLEDGMENTS

The authors would like to thank Qiang Zhao for useful discussions. We also thank B. Krusche and M. Dieterle for providing us the data of neutral pion photoproduction on the nucleons, Jan Hartmann for providing us the new data of polarization observables T, P, and H for the $\gamma p \to \pi^0 p$ reaction, and Paolo Levi Sandri for providing us the data on beam asymmetry for the $\gamma n \to \pi^0 n$ reaction. This work is supported, in part, by the National Natural Science Foundation of China (Grants No. 11075051, No. 11375061, and No. 11405222), and the Hunan Provincial Natural Science Foundation (Grant No. 13JJ1018).

[1] E. Klempt and J. M. Richard, Rev. Mod. Phys. **82**, 1095 (2010).
[2] B. Krusche and S. Schadmand, Prog. Part. Nucl. Phys. **51**, 399 (2003).
[3] M. Dieterle *et al.* (A2 Collaboration), Phys. Rev. Lett. **112**, 142001 (2014).
[4] M. Fuchs *et al.*, Phys. Lett. B **368**, 20 (1996).
[5] R. Beck, Eur. Phys. J. A **28**(Suppl. 1), 173 (2006).
[6] N. Sparks *et al.* (CBELSA/TAPS Collaboration), Phys. Rev. C **81**, 065210 (2010).
[7] H. van Pee *et al.* (CB-ELSA Collaboration), Eur. Phys. J. A **31**, 61 (2007).
[8] A. V. Anisovich, A. Sarantsev, O. Bartholomy, E. Klempt, V. A. Nikonov, and U. Thoma, Eur. Phys. J. A **25**, 427 (2005).
[9] O. Bartholomy *et al.* (CB-ELSA Collaboration), Phys. Rev. Lett. **94**, 012003 (2005).
[10] J. Hartmann, H. Dutz, A. V. Anisovich, D. Bayadilov, R. Beck, M. Becker, Y. Beloglazov, A. Berlin *et al.*, Phys. Rev. Lett. **113**, 062001 (2014).
[11] O. Bartalini *et al.* (GRAAL Collaboration), Eur. Phys. J. A **26**, 399 (2005).
[12] M. Dugger, B. G. Ritchie, J. P. Ball, P. Collins, E. Pasyuk, R. A. Arndt, W. J. Briscoe, I. I. Strakovsky *et al.*, Phys. Rev. C **76**, 025211 (2007).
[13] F. V. Adamian, A. Y. Bunyatyan, G. S. Frangulian, P. I. Galumian, V. H. Grabsky, A. V. Airapetian, H. H. Hakopian, V. K. Hoktanian *et al.*, Phys. Rev. C **63**, 054606 (2001).
[14] D. Elsner *et al.* (CBELSA and TAPS Collaborations), Eur. Phys. J. A **39**, 373 (2009).
[15] V. Crede *et al.* (CBELSA/TAPS Collaboration), Phys. Rev. C **84**, 055203 (2011).
[16] A. Thiel, A. V. Anisovich, D. Bayadilov, B. Bantes, R. Beck, Y. Beloglazov, M. Bichow, S. Bose *et al.*, Phys. Rev. Lett. **109**, 102001 (2012).
[17] M. H. Sikora, D. P. Watts, D. I. Glazier, P. Aguar-Bartolome, L. K. Akasoy, J. R. M. Annand, H. J. Arends, K. Bantawa *et al.*, Phys. Rev. Lett. **112**, 022501 (2014).
[18] M. Gottschall *et al.* (CBELSA/TAPS Collaboration), Phys. Rev. Lett. **112**, 012003 (2014).
[19] R. Di Salvo, A. Fantini, G. Mandaglio, F. Mammoliti, O. Bartalini, V. Bellini, J. P. Bocquet, L. Casano *et al.*, Eur. Phys. J. A **42**, 151 (2009).
[20] A. V. Anisovich, E. Klempt, V. A. Nikonov, M. A. Matveev, A. V. Sarantsev, and U. Thoma, Eur. Phys. J. A **44**, 203 (2010).
[21] A. V. Anisovich, R. Beck, E. Klempt, V. A. Nikonov, A. V. Sarantsev, and U. Thoma, Eur. Phys. J. A **48**, 15 (2012).
[22] A. V. Anisovich, V. Burkert, E. Klempt, V. A. Nikonov, A. V. Sarantsev, and U. Thoma, Eur. Phys. J. A **49**, 67 (2013).
[23] W. Chen, H. Gao, W. J. Briscoe, D. Dutta, A. E. Kudryavtsev, M. Mirazita, M. W. Paris, and P. Rossi *et al.*, Phys. Rev. C **86**, 015206 (2012).
[24] R. L. Workman, M. W. Paris, W. J. Briscoe, and I. I. Strakovsky, Phys. Rev. C **86**, 015202 (2012).
[25] R. L. Workman, W. J. Briscoe, M. W. Paris, and I. I. Strakovsky, Phys. Rev. C **85**, 025201 (2012).
[26] D. Drechsel, S. S. Kamalov, and L. Tiator, Eur. Phys. J. A **34**, 69 (2007).
[27] M. Shrestha and D. M. Manley, Phys. Rev. C **86**, 055203 (2012).
[28] F. Huang, M. Döring, H. Haberzettl, J. Haidenbauer, C. Hanhart, S. Krewald, U. G. Meißner, and K. Nakayama, Phys. Rev. C **85**, 054003 (2012).
[29] D. Rönchen, M. Döring, F. Huang, H. Haberzettl, J. Haidenbauer, C. Hanhart, S. Krewald, U.-G. Meißner *et al.*, Eur. Phys. J. A **50**, 101 (2014).
[30] H. Kamano, S. X. Nakamura, T.-S. H. Lee, and T. Sato, Phys. Rev. C **88**, 035209 (2013).
[31] V. Kuznetsov *et al.* (GRAAL Collaboration), Phys. Lett. B **647**, 23 (2007).
[32] I. Jaegle *et al.* (CBELSA Collaboration and TAPS Collaboration), Phys. Rev. Lett. **100**, 252002 (2008).
[33] I. Jaegle, B. Krusche, A. V. Anisovich, J. C. S. Bacelar, B. Bantes, O. Bartholomy, D. E. Bayadilov, R. Beck *et al.*, Eur. Phys. J. A **47**, 89 (2011).
[34] K. A. Olive *et al.* (Particle Data Group Collaboration), Chin. Phys. C **38**, 090001 (2014).
[35] R. Shyam and O. Scholten, Phys. Rev. C **78**, 065201 (2008).
[36] V. Shklyar, H. Lenske, and U. Mosel, Phys. Lett. B **650**, 172 (2007).
[37] M. Döring and K. Nakayama, Phys. Lett. B **683**, 145 (2010).
[38] X. H. Zhong and Q. Zhao, Phys. Rev. C **84**, 045207 (2011).
[39] A. V. Anisovich, E. Klempt, B. Krusche, V. A. Nikonov, A. V. Sarantsev, U. Thoma, and D. Werthmüller, Eur. Phys. J. A **51**, 72 (2015).
[40] A. V. Anisovich, I. Jaegle, E. Klempt, B. Krusche, V. A. Nikonov, A. V. Sarantsev, and U. Thoma, Eur. Phys. J. A **41**, 13 (2009).
[41] R. G. Moorhouse, Phys. Rev. Lett. **16**, 772 (1966).
[42] Q. Zhao and F. E. Close, Phys. Rev. D **74**, 094014 (2006).
[43] Z. P. Li, Phys. Rev. D **50**, 5639 (1994).
[44] Z. P. Li, Phys. Rev. C **52**, 1648 (1995).
[45] Z. P. Li, H. X. Ye, and M. H. Lu, Phys. Rev. C **56**, 1099 (1997).
[46] Q. Zhao, J. S. Al-Khalili, Z. P. Li, and R. L. Workman, Phys. Rev. C **65**, 065204 (2002).
[47] Q. Zhao, Z. P. Li, and C. Bennhold, Phys. Rev. C **58**, 2393 (1998).
[48] Q. Zhao, J. S. Al-Khalili, and C. Bennhold, Phys. Rev. C **64**, 052201 (2001).
[49] Q. Zhao, Z. P. Li, and C. Bennhold, Phys. Lett. B **436**, 42 (1998).
[50] Z. P. Li and B. Saghai, Nucl. Phys. A **644**, 345 (1998).

[51] B. Saghai and Z. P. Li, Eur. Phys. J. A **11**, 217 (2001).
[52] J. He, B. Saghai, and Z. P. Li, Phys. Rev. C **78**, 035204 (2008).
[53] J. He and B. Saghai, Phys. Rev. C **80**, 015207 (2009).
[54] X. H. Zhong and Q. Zhao, Phys. Rev. C **84**, 065204 (2011).
[55] X. H. Zhong, Q. Zhao, J. He, and B. Saghai, Phys. Rev. C **76**, 065205 (2007).
[56] X. H. Zhong and Q. Zhao, Phys. Rev. C **79**, 045202 (2009).
[57] X. H. Zhong and Q. Zhao, Phys. Rev. C **88**, 015208 (2013).
[58] L. Y. Xiao and X. H. Zhong, Phys. Rev. C **88**, 065201 (2013).
[59] N. Isgur and G. Karl, Phys. Rev. D **18**, 4187 (1978).
[60] N. Isgur and G. Karl, Phys. Lett. B **72**, 109 (1977).
[61] S. Capstick and N. Isgur, Phys. Rev. D **34**, 2809 (1986).
[62] G. F. Chew, M. L. Goldberger, F. E. Low, and Y. Nambu, Phys. Rev. **106**, 1345 (1957).
[63] R. L. Walker, Phys. Rev. **182**, 1729 (1969).
[64] C. G. Fasano, F. Tabakin, and B. Saghai, Phys. Rev. C **46**, 2430 (1992).
[65] R. Koniuk and N. Isgur, Phys. Rev. D **21**, 1868 (1980); **23**, 818 (1981).
[66] J. J. de Swart, Rev. Mod. Phys. **35**, 916 (1963); **37**, 326 (1965).
[67] A. J. G. Hey, P. J. Litchfield, and R. J. Cashmore, Nucl. Phys. B **95**, 516 (1975).
[68] C. S. An and B. Saghai, Phys. Rev. C **84**, 045204 (2011).
[69] S. Capstick and W. Roberts, Fizika B **13**, 271 (2004).
[70] T. Sato and T. S. H. Lee, Phys. Rev. C **54**, 2660 (1996).
[71] T. Sato and T. S. H. Lee, Phys. Rev. C **63**, 055201 (2001).
[72] S. Schumann, B. Boillat, E. J. Downie, P. Aguar-Bartolome, J. Ahrens, J. R. M. Annand, H. J. Arends, R. Beck *et al.*, Eur. Phys. J. A **43**, 269 (2010).
[73] D. O. Riska and G. E. Brown, Nucl. Phys. A **679**, 577 (2001).
[74] D. H. Saxon, R. D. Baker, K. W. Bell, J. A. Blissett, I. J. Bloodworth, T. A. Broome, J. C. Hart, A. L. Lintern *et al.*, Nucl. Phys. B **162**, 522 (1980).
[75] R. Beck *et al.*, Phys. Rev. Lett. **78**, 606 (1997).
[76] E. Mazzucato, P. Argan, G. Audit, A. Bloch, N. de Botton, N. d'Hose, J. L. Faure, M. L. Ghedira *et al.*, Phys. Rev. Lett. **57**, 3144 (1986).
[77] B. B. Govorkov *et al.*, Yad. Fiz. **4**, 507 (1966).
[78] G. Fischer, H. Fischer, G. Von Holtey, H. Kaempgen, G. Knop, P. Schulz, H. Wessels, W. Braunschweig *et al.*, Nucl. Phys. B **16**, 93 (1970).
[79] H. C. DeStaebler, E. F. Erickson, A. C. Hearn, and C. Schaerf, Phys. Rev. **140**, B336 (1965).
[80] Y. Hemmi, Y. Inagaki, T. Inagaki, A. Maki, K. Miyake, T. Nakamura, Tamura, J. Tsukamoto *et al.*, Phys. Lett. B **43**, 79 (1973).
[81] M. Yoshioka, A. Noda, M. Daigo, Y. Hemmi, R. Kikuchi, M. Minowa, K. Miyake, T. Nakamura *et al.*, Nucl. Phys. B **168**, 222 (1980).
[82] C. Bacci, G. Penso, G. Salvini, C. Mencuccini, A. Reale, V. Silvestrini, M. Spinetti, and B. Stella, Phys. Rev. **159**, 1124 (1967).
[83] G. Blanpied, M. Blecher, A. Caracappa, R. Deininger, C. Djalali, G. Giordano, K. Hicks, S. Hoblit *et al.*, Phys. Rev. C **64**, 025203 (2001).
[84] V. B. Ganenko, V. G. Gorbenko, Y. V. Zhebrovskii, L. Y. Kolesnikov, I. I. Miroshnichenko, A. L. Rubashkin, V. M. Sanin, P. V. Sorokin *et al.*, Yad. Fiz. **20**, 356 (1974).
[85] A. A. Belyaev, V. A. Getman, V. G. Gorbenko, V. A. Gushchin, A. Y. Derkach, Y. V. Zhebrovsky, I. M. Karnaukhov, L. Y. Kolesnikov *et al.*, Nucl. Phys. B **213**, 201 (1983).
[86] G. Knies, H. Oberlack, A. Rittenberg, A. H. Rosenfeld, M. Bogdanski, and G. Smadja, Phys. Rev. D **10**, 2778 (1974).
[87] G. Barbiellini, G. Bologna, G. Capon, G. De Zorzi, F. L. Fabbri, G. P. Murtas, G. Diambrini, G. Sette *et al.*, Phys. Rev. **184**, 1402 (1969).
[88] R. W. Zdarko and E. B. Dally, Nuovo Cimento A **10**, 10 (1972).
[89] A. S. Bratashevsky, A. I. Derebchinsky, A. A. Zybalov, O. G. Konovalov, A. S. Omelaenko, and A. E. Tenishev, Yad. Fiz. **32**, 667 (1980).
[90] D. E. Lundquist, R. L. Anderson, J. V. Allaby, and D. M. Ritson, Phys. Rev. **168**, 1527 (1968).
[91] E. D. Bloom, C. A. Heusch, C. Y. Prescott, and L. S. Rochester, Phys. Rev. Lett. **19**, 671 (1967).
[92] A. A. Belyaev, V. A. Getman, V. G. Gorbenko, V. A. Gushchin, A. Y. Derkach, Y. V. Zhebrovsky, I. M. Karnaukhov, L. Y. Kolesnikov *et al.*, Yad. Fiz. **35**, 693 (1982).
[93] R. Querzoli, G. Salvini, and A. Silverman, Nuovo Cimento **19**, 53 (1961).
[94] K. H. Althoff, D. Finken, N. Minatti, H. Piel, D. Trines, and M. Unger, Phys. Lett. B **26**, 677 (1968).
[95] N. V. Goncharov, A. I. Derebchinskii, A. A. Zybalov, O. G. Konovalov, A. E. Tenishev, S. G. Tonapetyan, and V. M. Khvorostyan, Zh. Eksp. Teor. Fiz. **64**, 401 (1973).
[96] A. S. Bratashevsky, A. A. Zybalov, S. P. Karasev, O. G. Konovalov, E. E. Korobova, A. S. Omelaenko, P. V. Sorokin, Y. O. Storozhenko *et al.*, Yad. Fiz. **42**, 658 (1985).
[97] S. Kato, T. Miyachi, K. Sugano, K. Toshioka, K. Ukai, M. Chiba, K. Egawa, T. Ishii *et al.*, Nucl. Phys. B **168**, 1 (1980).
[98] P. Blum, P. Brinckmann, R. Brockmann, P. Lutter, W. Mohr, and R. Sauerwein, Z. Phys. A **277**, 311 (1976).
[99] P. Blum, R. Brockmann, and W. Mohr, Z. Phys. A **278**, 275 (1976).
[100] M. Fukushima, N. Horikawa, R. Kajikawa, H. Kobayakawa, K. Mori, T. Nakanishi, C. O. Pak, S. Suzuki *et al.*, Nucl. Phys. B **136**, 189 (1978).
[101] P. S. L. Booth, L. J. Carroll, G. R. Court, P. R. Daniel, R. Gamet, C. J. Hardwick, P. J. Hayman, J. R. Holt *et al.*, Nucl. Phys. B **121**, 45 (1977).
[102] P. Feller, M. Fukushima, N. Horikawa, R. Kajikawa, K. Mori, T. Nakanishi, T. Ohshima, C. O. Pak *et al.*, Nucl. Phys. B **110**, 397 (1976).
[103] A. Ando *et al.*, Physik-Daten (1977) (unpublished).
[104] Y. Hemmi, T. Inagaki, R. Kikuchi, A. Maki, K. Miyake, T. Nakamura, A. Sasaki, N. Tamura *et al.*, Nucl. Phys. B **55**, 333 (1973).
[105] C. Bacci, R. Baldini-Celio, B. Esposito, C. Mencuccini, A. Reale, G. Sciacca, M. Spinetti, and A. Zallo, Phys. Lett. B **39**, 559 (1972).
[106] K. Kossert, M. Camen, F. Wissmann, J. Ahrens, J. R. M. Annand, H. J. Arends, R. Beck, G. Caselotti *et al.*, Eur. Phys. J. A **19**, 391 (2004).
[107] Z. P. Li and F. E. Close, Phys. Rev. D **42**, 2207 (1990).
[108] S. Capstick, Phys. Rev. D **46**, 2864 (1992).
[109] X. Cao, V. Shklyar, and H. Lenske, Phys. Rev. C **88**, 055204 (2013).
[110] V. Shklyar, H. Lenske, and U. Mosel, Phys. Rev. C **87**, 015201 (2013).
[111] T. Boika, V. Kuznetsov, and M. V. Polyakov, arXiv:1411.4375.